A miR-124-mediated post-transcriptional mechanism controlling the cell fate switch of astrocytes to induced-neurons

Elsa Papadimitriou[1], Paraskevi N. Koutsoudaki[1,&], Irini Thanou[1], Timokratis Karamitros[2,#], Dimitra Karagkouni[3,#], Dafni Chroni-Tzartou[4], Maria Gaitanou[5], Christos Gkemisis[1], Maria Margariti[1], Evangelia Xingi[6], Socrates J. Tzartos[4], Artemis G. Hatzigeorgiou[3], Dimitra Thomaidou[1,6,*]

Affiliations

[1]Neural Stem Cells and Neuroimaging Group, Department of Neurobiology, Hellenic Pasteur Institute
[2]Bioinformatics and Applied Genomics Unit, Department of Microbiology, Hellenic Pasteur Institute
[3]DIANA-Lab, Hellenic Pasteur Institute & Dept. of Computer Science and Biomedical Informatics, Univ. of Thessaly
[4]Laboratory of Molecular Neurobiology and Immunology, Department of Neurobiology, Hellenic Pasteur Institute
[5]Laboratory of Cellular and Molecular Neurobiology – Stem Cells, Department of Neurobiology, Hellenic Pasteur Institute
[6]Light Microscopy Unit, Hellenic Pasteur Institute
[#]equally contributing authors
[&]Present address: Molecular Carcinogenesis Group, Department of Histology and Embryology, Medical School, National and Kapodistrian University of Athens, Athens, Greece

[*]**Corresponding author**
Email: thomaidou@pasteur.gr

Running title: miR-124-mediated neurogenic reprogramming of astrocytes

Keywords: astrocytes / direct reprogramming / ISX9 / miR-124 / Zfp36l1

Abstract

The miRNA miR-124 has been employed supplementary to neurogenic TFs and other miRNAs to enhance direct neurogenic conversion by suppressing multiple non-neuronal targets. Aim of the study was to investigate whether miR-124 is sufficient to drive direct reprogramming of astrocytes to induced-neurons (iNs) on its own and elucidate its independent mechanism of reprogramming action. Our data show that miR-124 is a potent driver of the reprogramming switch of astrocytes towards an immature neuronal fate, by directly targeting the RNA-binding protein Zfp36l1 implicated in ARE-mediated mRNA decay and subsequently de-repressing Zfp36l1 neurogenic interactome. To this end miR-124 contribution in iNs' production largely recapitulates endogenous neurogenesis pathways, being further enhanced upon addition of the neurogenic compound ISX9, which greatly improves both miR-124-induced reprogramming efficiency and iNs' functional maturation. Importantly, miR-124 is potent to guide direct conversion of reactive astrocytes to immature iNs of cortical identity *in vivo* following cortical trauma, confirming its 'master' reprogramming capacity within the injured cortical microenvironment, while ISX9 supplementation confers a survival advantage to newly produced iNs.

46 ## Introduction

47 Direct astrocytic reprogramming to induced-neurons (iNs) is a powerful approach for
48 manipulating cell fate, as it takes advantage of the intrinsic neural stem cell (NSC) potential of
49 reactive astrocytes (Magnusson et al. 2014), while it offers the possibility of reprogramming
50 resident brain cells. To this end astrocytic cell fate conversion to iNs has been well-established
51 *in vitro* (Berninger et al. 2007; Heinrich et al. 2010; Aravantinou-Fatorou et al. 2015)and *in*
52 *vivo* (Guo et al. 2014; Torper et al. 2013; Mattugini et al. 2019) using combinations of
53 transcription factors (TFs) or chemical cocktails (L. Zhang et al. 2015; Li et al. 2015; L. Gao et
54 al. 2017). Challenging the expression of lineage-specific TFs during reprogramming is
55 accompanied by changes in the expression of regulatory RNAs, mostly miRNAs, that post-
56 transcriptionally modulate high numbers of neurogenesis-promoting factors and to this end
57 miRNAs have been introduced, supplementary or alternatively to TFs, to instruct direct
58 neuronal reprogramming (Yoo et al. 2011).

59 Among neurogenic miRNAs, miR-124 has been shown to contribute to efficient neurogenic
60 conversion of fibroblasts when coupled with certain TFs or other miRNAs, in particular miR-
61 9/9* and the strong neuronal reprogramming potential of this cocktail has been elaborately
62 studied at the transcriptomic and epigenetic level (Ambasudhan et al. 2011; Abernathy et al.
63 2017; Wohl and Reh 2016; Victor et al. 2014). miR-124 acts globally to increase the expression
64 levels of neuronal genes by repressing components of major neuronal gene repressor
65 complexes, such as the anti-neural transcriptional repressor REST complex (Visvanathan et al.
66 2007; Baudet et al. 2012; Volvert et al. 2014) and the Polycomb Repressive Complex 2 (PRC2)
67 (Neo et al. 2014; Lee et al. 2018), while it also participates at the post-transcriptional
68 regulation of neuronal transcripts by targeting the neuron-specific splicing global repressor
69 Ptbp1 (Makeyev et al. 2007). Besides its roles in transcriptional and post-transcriptional
70 regulation, miR-124 is a key mediator of a chromatin permissive environment for neuronal
71 reprogramming through its involvement in the formation of the neuron specific chromatin
72 remodeling complex nBAF (Yoo et al. 2009).

73 However, although miR-124 has been lately utilized in many reprogramming cocktails for the
74 neurogenic conversion of fibroblasts (Birtele et al. 2019; Jiang et al. 2015; Victor et al. 2018;
75 Ambasudhan et al. 2011; Yoo et al. 2011), neither its potential to induce fate conversion of
76 astrocytes to induced-neurons (iNs) *in vitro* or *in vivo*, nor its mechanism of action in
77 instructing direct reprogramming on its own have been investigated. In this study we show
78 that miR-124 is sufficient to instruct reprogramming of cortical astrocytes to immature iNs *in*

79 *vitro* controlling the reprogramming "switch" of astrocytes towards the neuronal fate by
80 down-regulating genes with important regulatory roles in astrocytic function. Among these
81 we identified for the first time the RNA binding protein Zfp36l1, implicated in ARE-mediated
82 mRNA decay (Lai et al. 2000), as a direct target of miR-124 and further found certain neuronal-
83 specific Zfp36l1 targets that participate in cortical development being de-repressed in miR-
84 124-iNs. Importantly, by blocking miR-124 specific binding in Zfp36l1 3'UTR, we revealed that
85 miR-124/Zfp36l1 interaction is one of the drivers of miR-124-induced astrocytic fate switch
86 and induction of neuronal identity. To enhance the neuronal differentiation of reprogrammed
87 immature iNs, we combined miR-124 with isoexasole-9 (ISX9) chemical compound known to
88 possess neurogenesis-promoting properties (Schneider et al. 2008; Li et al. 2015). Functional
89 analysis of the two molecules' combination revealed that *in vitro* addition of ISX9 promoted
90 both the neurogenic conversion and greatly enhanced the functional maturation of miR-
91 124+ISX9-iNs. Importantly, *in vivo* miR-124 was also potent either alone or along with ISX9, to
92 guide neuronal reprogramming of reactive astrocytes following cortical trauma to immature
93 iNs, present after 8 weeks, with ISX9 contributing to iNs' enhanced survival, revealing the *in*
94 *vivo* 'master' reprogramming capacity of miR-124 within the injured cortical micro-
95 environment.

96 # Results

97 **miR-124 is sufficient to instruct reprogramming of postnatal cortical astrocytes to immature**
98 **induced- neurons**

99 To study the potential of miR-124 to instruct neuronal reprogramming of astrocytes on its
100 own, cultured postnatal day3-5 (P3-5) mouse cortical astrocytes were transfected with miR-
101 124-3p mimics (**Fig 1A**). Firstly, we verified that the initial primary astrocytic culture comprised
102 majorly of GFAP+ astrocytes (72.2% ± 8.6%), while only 2.3%± 2.1%were Tuj1+ neurons (**Suppl**
103 **Fig 1A and B**). BrdU administration for the first 4 days of reprogramming revealed that about
104 70% of cells at day7 (d7) (astrocytes treated or not with scrambled miRNA, sc-miRNA) had
105 undergone cell division, while overexpression of miR-124 significantly reduced this percentage
106 to 50% (**Suppl Fig 1D and E**). After 1 week (d7) nearly 35% of miR-124-treated cells were Tuj1+,
107 exhibiting multipolar morphology **(Fig 1B and C)**, as compared to control astrocytes that
108 received sc-miRNA, where no Tuj1positivity was detected (**Suppl Fig 1C**). Still, miR-124-iNs
109 exhibited low differentiation potential and only 19% of the cells remained Tuj1+ at d14 of the
110 reprogramming process (**Fig 1B and C**). Notably almost 60% of Tuj1+ miR-124-iNs at d7 had
111 incorporated BrdU (**Supl Fig 1F**), accounting for nearly 20% of the total cells in culture (**Suppl**
112 **Fig 1G**), indicating their non-neuronal origin. The ability of miR-124 to instruct neurogenic
113 reprogramming was further supported by RT-qPCR expression analysis of several neurogenic
114 transcription factors (TFs) at d7, where miR-124 overexpression induced the up-regulation of
115 the mRNA levels of the proneural TFs *Mash1* and to a lesser extend *Neurog2* (**Fig 1D**), while it
116 additionally up-regulated TFs related to both dorsal (*Tbr2, Tbr1, Fezf2* and *Cux1*) (**Fig 1E**) and
117 ventral telencephalon development (*Gsx2, Dlx1*) (**Fig 1F**). We also observed up-regulation of
118 TFs related to neuronal differentiation (*Sox4, Sox11, Hes6*) (**Fig 1G**), however we failed to
119 detect an up-regulation of *NeuroD1* (**Fig 1G**), which is known to play a crucial role in neuronal
120 reprogramming (Pataskar et al. 2016; Matsuda et al. 2019; Guo et al. 2014). Instead, miR-124
121 significantly reduced *NeuroD1* mRNA levels, implying that this reduction may contribute to
122 the low differentiation capacity of miR-124-iNs. Further, immunofluorescence analysis
123 indicated that the majority of miR-124-iNs (nearly 80%) were Mash1+ and also exhibited low
124 Tbr2 expression (nearly 70%), while only a small percentage of reprogrammed cells (15%)
125 were positive for the ventral TF Gsx2 (**Fig 1H and I**), indicating that the Mash1-Tbr2 trajectory
126 is most prominently activated in the majority of miR-124-iNs.

127

128 **The neurogenic compound ISX9 greatly enhances the miR-124-induced reprogramming**
129 **efficiency and differentiation state of iNs**

130 The observed down-regulation of NeuroD1 by miR-124 prompted us to supplement the
131 reprogramming medium from d2 to d10 with the chemical compound ISX9, known to up-
132 regulate NeuroD1 levels and enhance neuronal differentiation (Schneider et al. 2008). Indeed,
133 ISX9 addition led to the acquisition of a more differentiated neuronal phenotype with a
134 smaller soma and longer projections (**Fig 2A**) and significantly increased the percentage of
135 Tuj1+ iNs from 35% to 62% at d7 and from 19% to 38% at d14 (**Fig 2B**). Importantly, ISX9 was
136 potent to reverse the miR-124-induced reduction of *NeuroD1* mRNA levels (**Fig 2C**) and to
137 greatly elevate the transcriptional levels of *Neurog2* and *Tbr2* peaking at d7 (**Fig 2D**), while it
138 also induced a moderate reduction in *Mash1* mRNA levels (**Fig 2E**). Importantly, ISX9 was not
139 able to induce reprogramming of astrocytes on its own (sc-miRNA+ISX9) (**Suppl Fig 2A**),
140 despite evoking robust up-regulation of the mRNA levels of *NeuroD1* (**Fig 2D**) and other
141 neurogenic TFs (**Suppl Fig 2B**) and to a small, but significant, extend the protein levels of
142 Mash1 and Tbr2 (**Suppl Fig 2C and D**). Additionally, supplementation of ISX9 along with miR-
143 124 significantly increased the percentage of Tbr2+/Tuj1+ iNs, without affecting the
144 percentages of Mash1+/Tuj1+ iNs or Gsx2+/Tuj1+ iNs relatively to miR-124 alone (**Fig 2F and**
145 **G**). Still, measurement of the mean nuclear fluorescence intensity per cell in miR-124-iNs and
146 miR-124+ISX9-iNs at d7, revealed a significant enhancement of Tbr2 protein levels (**Fig 2H**)
147 and a down-regulation of Mash1 levels (**Fig 2I**) following ISX9 addition.

148 These results led us to the inference that addition of ISX9 in the reprogramming medium
149 reinforces the passage of miR-124+ISX9-iNs through a Tbr2+ intermediate stage, which seems
150 to be the main reprogramming route these iNs follow. Interestingly, the addition of ISX9 also
151 significantly enhanced the expression of *Insm1* (**Suppl Fig 2E**), a key transcriptional regulator
152 of intermediate progenitors (IPs) (Elsen et al. 2018), further supporting the notion that iNs
153 pass through an intermediate stage bearing molecular characteristics of endogenous IPs.

154

155 **miR-124+ISX9-iNs exhibit characteristics of mature, electrophysiologically active neurons**

156 The majority of miR-124-iNs and miR-124+ISX9-iNs were positive for the cortical TF Tbr1 at
157 d14 (**Suppl Fig 3A and B**). We mainly observed a moderate nuclear Tbr1 expression in miR-
158 124-iNs, whereas miR-124+ISX9-iNs exhibited strong cytoplasmic Tbr1 expression, besides a
159 moderate nuclear one (**Suppl Fig 3A**), a finding that has been previously reported in cortical
160 neurons (Hong and Hsueh 2007). After 21d in culture, nearly 80% of Tuj1+ miR-124+ISX9-iNs

161 were also positive for the mature neuronal markers MAP2 and Synapsin1, exhibiting a
162 differentiated neuronal morphology (**Fig 3A and B**), while miR-124-iNs at d21 did not exhibit
163 signs of further maturation and only a small percentage of them were MAP2+ and Synapsin1+
164 (**Fig 3B**). Additionally, at d28 the majority of miR-124+ISX9-iNs (nearly 90%) were positive for
165 the glutamatergic marker vGlut1 (**Fig 3C and D**), while only 12% of them were positive for
166 GABA (**Fig 3D and Suppl Fig 3C**).

167 To further establish the functional maturation of miR-124-iNs and miR-124+ISX9-iNs we
168 performed electrophysiological analysis with whole-cell voltage-clamp and current-clamp
169 recordings at different time points from d15 to d27. Rapidly inactivating inward Na^+ currents
170 and persistent outward K^+ currents were recorded in miR-124+ISX9-iNs after d22 (n=47 out of
171 80 analyzed cells) in response to depolarizing voltage steps (**Fig 3E, left panel, Fig 3F**), while
172 further application of TTX and TEA – selective Na^+ channels' (Na_V) and K^+ channels' (K_V)
173 blockers respectively – confirmed that the Na_V were responsible for the inward currents and
174 K_V for the outward currents (**Fig 3E, middle and right panels**). A small amount of K_V channels
175 appeared in miR-124+ISX9-iNs before d21, while they became more evident in d23-27 **(Fig 3F)**,
176 in accordance with the ability of almost all recorded miR-124+ISX9-iNs (n=21 out of 30
177 recorded cells) to generate repetitive action potentials (APs) upon membrane depolarization
178 (**Fig 3G**). Finally, rare spontaneous post-synaptic current activity was detected in few mature
179 miR-124+ISX9-iNs (d27) (**Fig 3H**).On the other hand, miR-124-iNs exhibited lower amounts of
180 Na_v and K_v channels and were thus not capable of firing action potentials (APs) (n=15cells).

181 The majority (80%) of miR-124+ISX9-iNs (**Fig 3I**) were capable of responding to different
182 concentrations of GABA early in the course of their maturation (d22), even before the
183 appearance of APs, which is in compliance with the expression of GABA receptors in early
184 stages of neuronal development (Luján, Shigemoto, and López-Bendito 2005). Additionally,
185 miR-124+ISX9-iNs were capable of responding to L-glutamate in a concentration dependent
186 manner (**Fig 3J**), while L-glutamate-sensitive inward current was completely blocked after co-
187 application of 100μM L-glutamate and 20μM CNQX, indicating the presence of AMPA/kainite
188 receptors (**Fig 3K**).

189 **miR-124 and ISX9 exhibit both independent and cooperative transcriptional contributions**
190 **in the reprogramming process to iNs**

191 To in-depth analyze the molecular mechanism through which miR-124 contributes to the
192 reprogramming process either alone or following ISX9 supplementation, we performed RNA-
193 sequencing of miR-124-iNs and miR-124+ISX9-iNs at d7, using as controls astrocytes obtained

194 the initial day of the reprogramming (d1) and sc-miRNA transfected astrocytes at d7. The
195 differential expression analysis was performed between d7 miR-124-iNs or miR-124+ISX9-iNs
196 and d1 astrocytes (astro) to uncover the whole spectrum of transcriptional changes occurring
197 during neurogenic reprogramming of initiating astrocytes (miR-124-iNs *vs* astro and miR-
198 124+ISX9-iNs *vs* astro respectively), whereas the d7 sc-miRNA-transfected astrocytes (sc-
199 miRNA astro) were used the ultimate control for the identification of miR-124 target genes
200 (see **Fig 5** below).

201 We identified 4,233 differentially expressed genes (DEGs) in miR-124-iNs *vs* astro and 6,652
202 DEGs in miR-124+ISX9-iNs *vs* astro ($1 \leq \log_2$(fold change)≤ -1, FDR<0.05) (**Suppl Fig 4A**). Heat
203 map analysis of DEGs (miR-124-iNs *vs* astro and miR-124+ISX9-iNs *vs* astro) belonging to the
204 GO terms: Glial cell differentiation, Gliogenesis, Astrocyte development, Generation of
205 neurons, Neuron differentiation, Regulation of neuron differentiation, Neurotransmitter
206 transport and Synaptic signaling (**Fig 4A**) indicated that miR-124 alone efficiently down-
207 regulated a gene cluster enriched in astrocytic genes (**Cluster I**). At the same time miR-124 up-
208 regulated a gene cluster of neuronal specific genes (**Cluster III**) many of which were further
209 up-regulated by ISX9 supplementation, while ISX9 highly up-regulated a neuronal specific
210 gene cluster (**Cluster II**) that was most exclusively expressed in miR-124+ISX9-iNs.

211 GO enrichment analysis of biological processes for the up-regulated DEGs of both miR-124-
212 iNs *vs* astro and miR-124+ISX9-iNs *vs* astro, further revealed that miR-124 alone up-regulated
213 genes related to generation of neurons and neuronal differentiation as well as to more specific
214 neuronal functions mostly associated to synaptic transmission (**Fig 4B in orange**), while ISX9
215 greatly enhanced the number of up-regulated genes related to more mature neuronal
216 functions such as action potential, axon development and subtype specific synaptic
217 transmission (**Fig 4B in red**). Furthermore, enrichment analysis of the down-regulated DEGs
218 of miR-124-iNs *vs* astro indicated that many of them were related to cell cycle, gliogenesis,
219 and astrocyte differentiation (**Fig 4C**). Interestingly, this analysis revealed a strong effect of
220 miR-124 in down-regulating components of many signaling pathways, including MAPK, PKB,
221 canonical Wnt, TGF-β, BMP, Notch and JAK/Stat signaling pathways (**Fig 4C**), known to play
222 important roles in astrocytic identity and function (Gross et al. 1996; Acaz-Fonseca et al. 2019;
223 Kang and Hébert 2011; Yang et al. 2012).

224 Since reprogramming is a process that implicates great changes in the transcriptomic, post-
225 transcriptomic and epigenetic landscape of trans-differentiating cells, we sought to identify
226 the differentially expressed transcription factors (TFs), epigenetic factors (EFs) and RNA
227 binding proteins (RBPs) in our datasets that could possibly drive the reprogramming process.

228 Heat map analysis of astrocytic TFs (**Suppl Fig 4B**) indicated that miR-124 potently down-
229 regulated TFs related to astrocytic function such as *Id1, Id3, Tcf4, Tcf7l1, Rbpj* and *Nfic,* while
230 the addition of ISX9 exhibited minor contribution to their down-regulation (**Suppl Fig 4B**).
231 Importantly, validation of many of those genes with RT-qPCR verified the observed trend and
232 also indicated that ISX9 alone (sc-miRNA+ISX9) failed to down-regulate their mRNA levels
233 (**Suppl Fig 4C**). In parallel, heat map analysis of up-regulated neuronal-specific TFs revealed
234 that miR-124 up-regulated TFs related to telencephalon development such as *Tox, Foxo6,*
235 *Scrt1, Scrt2* and *Rcor2* (**Fig 4D**), along with TFs that we had already identified through prior
236 qRT-PCR analysis (*Mash1, Insm1, Hes6, Sox4, Fezf2, Gsx2, Dlx1*). Additionally, ISX9 increased
237 the number of TFs implicated in telencephalon development, among which *Eomes (Tbr2),*
238 *Prdm8, Ovol2, Tfap2c* and *Tshz2* (**Fig 4D**), but unexpectedly it also highly up-regulated TFs
239 related to more ventral/caudal brain regions, such as the retina, midbrain, hindbrain/spinal
240 cord (**Fig 4D**), possibly implying that ISX9 expands region-specific neuronal identity at the
241 transcriptional level. Validation of selected TFs/EFs expressed either in telencephalon (**Suppl**
242 **Fig 4D**) or midbrain (**Suppl Fig 4E**) and hindbrain/spinal cord (**Suppl Fig 4F**) by RT-qPCR verified
243 their up-regulation by ISX9.

244 Interestingly, heat map analysis of differentially expressed RNA-binding proteins (RBPs)
245 revealed that miR-124 was sufficient to down-regulate many RBPs expressed in astrocytes
246 such as the splicing factors *Ptbp1, Snrpa1, Lgals3* and *Isy1* and the mRNA decay proteins *Zfp36,*
247 *Zfp36l1, Zfp36l2* (**Fig 4E**). In addition, miR-124 moderately up-regulated neuronal specific
248 RBPs, among which *Elavl2, Elavl4, Nova1, Rbfox1, Rbfox2, Celf3* and *Nol3,* while ISX9 induced
249 their further up-regulation and significantly increased the number of neuron specific RBPs
250 such as *Aplp1, Celf4, Celf5, Celf6, Elavl3, Ern2, Esrp2* and *Rbfox3* (**Fig 4E**).

251 The analysis of differentially expressed EFs revealed that miR-124 increased the levels of
252 several EFs related to epigenetic transcriptional activation, including *Kmt2c*, *Tet1*, *Smarca1,*
253 *Smarca2, Chd7* and *Ss18l1 (Crest)* (**Suppl Fig 4G**). On the other hand ISX9 further contributed
254 in up-regulating *Chd5, Actl6b*, *Dpf3* and *Smyd3*, while interestingly it majorly contributed in
255 down-regulating EFs related to epigenetic transcriptional repression, such as *Suv39h1*,
256 *Suv39h2*, *Hdac5* and *Hdac7* (**Suppl Fig 4G**).

257 The above observations led us conclude that miR-124 is sufficient to induce the astrocytic
258 reprogramming switch towards an immature cortical neuronal fate through down-regulation
259 of many glial-specific genes, many of which exhibit important regulatory functions. ISX9, on
260 the other hand, acts auxiliary by enhancing neuronal-specific gene transcription contributing
261 to the maturation of miR-124 immature-iNs.

262 **The non-neuronal RBP Zfp36l1 is a novel direct target of miR-124**

263 To get a closer insight into the post-transcriptional effects of miR-124 on the astrocytic
264 transcriptome, we sought to determine the direct targets of miR-124 that could act as drivers
265 of the reprogramming switch. For this, we utilized publicly available AGO-HITS-CLIP data
266 performed in mouse brain cortex (Chi et al. 2009) in order to detect miR-124 binding sites.
267 The analysis revealed 171 miR-124 direct targets that were also defined as down-regulated in
268 the miR-124-iNs *vs* sc-miRNA astro RNA-Seq analysis ($\log_2$(fold change)≤-1, FDR<0.01). miR-
269 124 targets were subsequently filtered to examine genes expressed in astrocytes, utilizing a
270 published reference list for expressed transcripts in distinct cell types of the mouse brain (Y.
271 Zhang et al. 2014), ending up with 130 miR-124 direct target genes (**Fig 5A**). Interestingly,
272 among these genes we identified the known targets of miR-124, Sox9 and Lhx2, but failed to
273 detect Ptbp1 and Scp1, which are well characterized miR-124 targets with prominent role in
274 neurogenic reprogramming.

275 In search of novel miR-124 targets with regulatory role, a prominent target was the RBP
276 Zfp36l1, implicated in the mRNA decay (Lai et al. 2000) and highly expressed in cortical glial
277 cells (Weng et al. 2019), cortical radial glial precursors (Yuzwa et al. 2017; Weng et al. 2019)
278 and other non-neuronal cells (Carrick and Blackshear 2007). miR-124 directly binds to the 3'
279 UTR of Zfp36l1 transcript with perfect seed complementarity (7mer-m8 site) (**Fig 5B**), while in
280 re-analysis of publicly available AGO-HITS-CLIP data from human motor cortex and cingulate
281 gyrus tissues, the miR-124 binding site on the 3' UTR of ZFP36L1 human transcript was found
282 to be conserved (**Fig 5B**).

283 The targeting of this binding site in Zfp36l1 3'UTR by miR-124 was further validated by
284 luciferase assays, where it was shown that its mutation completely blocked the strong down-
285 regulation of luciferase activity induced by miR-124 (**Fig 5C, Suppl Fig 5A and B**). Of note, miR-
286 124 does not target the 3'UTR of Zfp36l2, predicted to contain 2 binding sites (**Fig 5C and**
287 **Suppl Fig 5C and D**), further supporting its specificity on Zfp36l1 regulation. The efficient
288 down-regulation of *Zfp36l1* by miR-124 was also validated by RT-qPCR, revealing that it is a
289 very early event in the course of reprogramming (**Suppl Fig 5E**). Interestingly, ISX9 was not
290 potent to down-regulate *Zfp36l1* mRNA levels (**Fig 5D**), further supporting our initial
291 observation that ISX9 alone cannot instruct reprogramming of astrocytes to iNs, possibly by
292 failing to down-regulate astrocytic genes.

293 Since Zfp36l1 acts by mediating degradation of its mRNA targets, we were interested in
294 identifying Zfp36l1 mRNA targets, being up-regulated in our analysis. For this purpose, we

295 combined two publicly available Zfp36l1 iCLIP-Seq data from thymocytes (Vogel et al. 2016)
296 and B lymphocytes (Galloway et al. 2016) and ended up with 621 Zfp36l1 direct targets that
297 are up-regulated in miR-124-iNs *vs* sc-miRNA astro (log_2(fold change)≥1, FDR<0.05), which
298 importantly correspond to 47% of miR-124 up-regulated DEGs. GO enrichment analysis
299 revealed that many of these genes are implicated in neurogenesis, neuron projection
300 development, synaptic transmission, axonogenesis, dendritic morphogenesis and
301 telencephalon development (**Fig 5E**). Interestingly, many of them were also found to regulate
302 transcription and RNA processing (**Fig 5E**), highlighting an important regulatory role for many
303 Zfp36l1 targets with possible impact on the reprogramming process. Among these targets we
304 found neurogenic TFs, such as *Tox, Tox3, Rcor2, Cux1, Hes6, Lzts1* and *Mllt11*and EFs related
305 to neurogenesis such as *Chd3, Chd7, Kmt2c* and *Tet1* (**Fig 5F**). Notably, we also identified as
306 Zfp36l1 targets the neuronal RBPs *Elavl4, Nova1* and *Rbfox1* (**Fig 5F**). This constitutes a
307 significant finding that suggests the repression of neuronal RBPs' directly by Zfp36l1, being
308 relieved upon miR-124-mediated Zfp36l1 down-regulation.

309 We subsequently examined the mRNA levels of the Zfp36l1 targets identified by our analysis,
310 *Elavl*4, *Nova1, Rbfox1, Rcor2* and *Tox* upon miR-124 overexpression with RT-qPCR and verified
311 that miR-124 was potent to induce their up-regulation (**Fig 5G**). We also verified the increase
312 of the protein levels of the neurogenic TF, Tox, in miR-124-iNs at d5 (**Suppl Fig 5F and G**).
313 Notably, we observed that the combination of miR-124 with ISX9 greatly further enhanced
314 the mRNA levels of the RBP identified as targets of Zfp36l1, *Elavl4* and *Rbfox1* (**Suppl Fig 5H**),
315 as well as the other neuronal RBPs of the nElavl family, *Elavl2* (**Suppl Fig 5I**) and *Elavl3* (**Suppl**
316 **Fig 5J**), highlighting the importance of ISX9 in reinforcing and supplementing the neurogenic
317 action of miR-124.

318 Collectively, these data show that the identified here targets of Zfp36l1 correspond to half of
319 the miR-124-up-regulated genes and many of them constitute neuronal-specific genes with
320 important regulatory functions. Thus the miR-124/Zfp36l1 interaction bears the potential to
321 play a key regulatory role in the control of the neurogenic reprogramming switch of astrocytes
322 by miR-124.

323 **Targeting of Zfp36l1 by miR-124 plays a key role in the miR-124-induced cell fate switch of**
324 **astrocytes to iNs**

325 To investigate the impact of the miR-124/Zfp36l1 interaction on the miR-124-mediated
326 reprogramming of astrocytes, we used a target site blocker (TSB) oligonucleotide that
327 competitively binds to miR-124 binding site on the 3' UTR of Zfp36l1 mRNA, blocking its down-

328 regulation by the miR-124-RISC complex (**Fig 6A**). The moderate down-regulation of Zfp36l1
329 protein by miR-124 as early as d5 of reprogramming was reversed by TSB at the miR-124:TSB
330 molecular ratio 2:1, as estimated by western blot (**Fig 6B and C**), while we observed no
331 significant effect of TSB on Zfp36l2 protein levels (**Suppl Fig 6A and B**). Due to extensive stress
332 and cell death, the effect of TSB on the reversal of Zfp36l1 protein levels upon miR-124 over-
333 expression was not possible to be estimated for a longer time point of the reprogramming.

334 Next, we tested the effect of TSB on the mRNA levels of the identified neuronal targets of
335 Zfp36l1, *Tox, Rbfox1, Nova1, Rcor2* and *Elavl4* by RT-qPCR initially at d3 and observed a dose-
336 dependent reduction of the miR-124-induced up-regulation of *Tox, Rbfox1, Nova1* and *Rcor2*,
337 but not of *Elavl4*, in the presence of increasing concentrations of TSB (miR-124:TSB molecular
338 ratio 4:1, 2:1 and 1:1) (**Fig 6D**). The mRNA levels of *Tox* and *Rbfox1* retained the same response
339 to TSB at a later time point, at d5 (**Suppl Fig 6C and D**), an effect that was not observed for
340 *Nova1*, *Rcor2* and *Elavl4* (**Suppl Fig 6E**), implying that their post-transcriptional regulation
341 becomes more complex as the neuronal conversion is gradually established. Importantly, TSB
342 resulted in a significant and dose-dependent reduction in the percentage of Tuj1+ miR-124-
343 iNs at d5 (**Fig 6E and F**), with an evident alteration of their characteristic immature neuronal
344 morphology (**Fig 6E and G**). More specifically, morphological analysis of the number of
345 processes extending from the soma and the size of the soma of Tuj1+ cells indicated that TSB
346 addition resulted in gradual abolishment of their multipolar morphology with fine processes,
347 characteristic of miR-124-iNs (**Fig 6E left panel and G**) and instead largely led to the retention
348 of a premature astrocyte-like morphology with bigger soma (**Suppl Fig 6F**) and none or very
349 few processes (**Fig 6E right panel and G**).

350 These observations strongly indicate that the targeting of Zfp36l1 by miR-124 is an important
351 event during the miR-124-induced reprogramming by unlocking neurogenic genes with
352 important regulatory activity and by controlling the necessary morphological changes.

353 **miR-124 induces reprogramming of resident reactive astrocytes to immature iNs *in vivo***
354 **following cortical trauma**

355 To evaluate the *in vivo* reprogramming potential of miR-124 to drive cell fate conversion of
356 resident reactive cortical astrocytes to iNs alone or in synergy with ISX9, we applied two viral-
357 based approaches (using lentiviral and AAV vectors) to overexpress miR-124 into the
358 mechanically injured cortex of 3-4 months old mice. In the lentiviral transfer approach, we
359 stereotaxically injected either control LV-GFP or LV-miR-124-GFP to transduce reactive
360 astrocytes surrounding the cortical injury site, while ISX9 was systemically administered for 5

361 consecutive days beginning 2 days after viral injection (p.i.) in a group of mice (**Fig 7A**). Seven
362 days p.i. the majority of transduced cells surrounding the injury site (**Suppl Fig 7A**) in both
363 conditions were GFAP+ reactive astrocytes (71.6% ± 8.0% for LV-GFP and 65.7% ± 15.7% for
364 LV-miR-124-GFP), while the percentage of transduced NeuN+ neurons was much lower (6.4%
365 ± 3.6% for LV-GFP and 15.3% ± 3.7% for LV-miR-124-GFP) (**Suppl Fig 7B**). Analysis of
366 NeuN+/GFP+ transduced cells 3weeks (3w) p.i. revealed that 71.8% ± 12.4% of the LV-miR-
367 124-transduced cells were NeuN+, while only 10.2% ± 2.6% of the LV-GFP transduced cells
368 were NeuN+ exhibiting no significant difference between the 7d and 3w time points (**Fig 7B**
369 **and C**). These results point to a strong potential of miR-124 to drive direct conversion of
370 reactive astrocytes into iNs *in vivo*, while the administration of ISX9 showed no further
371 significant contribution to this conversion (**Fig 7C**). The vast majority of NeuN+ iNs in both
372 groups were also positive for the cortical marker Tbr1 (98% ± 4.1% for LV-miR-124-GFP and
373 88% ± 11.1% for LV-miR-124-GFP+ISX9) (**Suppl Fig 7C and D**).

374 To further validate the astrocytic origin of iNs upon miR-124 force-expression in the same
375 cortical trauma model, supplementary to the lentiviral approach we employed a viral lineage
376 tracing strategy by stereotaxically co-injecting AAV5-GFAP-Cre virus, to mark cortical
377 astrocytes, along with AAV9-CMV-miR-124-mCherry virus to overexpress miR-124 in the cells
378 of the injured cortex of R26R-EYFP reporter mice (**Fig 7D**). However we observed unexpected
379 GFP expression in peritraumatic resident neurons besides its expression in astrocytes as early
380 as 7d after AAV5-GFAP-Cre injection, indicating that in accordance with recent reports (Wang
381 et al. 2021), this approach cannot warranty exclusive astrocytic lineage tracing. Given this
382 limitation, we restricted our analysis to the AAV9-CMV-miR-124-expressing cells, also
383 employing BrdU administration to label the proliferating astrocytes' population of the
384 peritraumatic area. Analysis of the cell type of AAV9-miR-124-transduced cells 7d p.i. revealed
385 that their majority was GFAP+ reactive astrocytes (92.5% ± 4.2%), with only 9.5% ± 2.1% being
386 NeuN+ neurons (**Fig 7E and Suppl Fig 8A**), while 3w later 42.8% ± 7.8% of them were NeuN+
387 iNs, exhibiting an immature neuronal morphology (**Fig 7F and G, Suppl Fig 9B**). ISX9
388 administration along with miR-124 led to a small, not statistically significant increase in NeuN+
389 iNs' percentage (51.6% ± 7.5%) (**Fig 7G**), without further affecting their morphology. In
390 accordance with the lentiviral approach, in both conditions the percentage of Tbr1+ iNs was
391 almost equal to that of NeuN+ iNs (41.2% ± 3.6% in AAV9-miR-124 and 51.4% ± 15.4% in AAV9-
392 miR-124+ISX9) (**Suppl Fig 8B**). Further analysis at the longer time point of 8w revealed that
393 the percentage of NeuN+ iNs increased to 74.5% ± 2.6% (**Fig 7G**), with a small but statistically
394 significant additional increase (79.4% ± 0.8%) in AAV-miR-124+ISX9 (**Fig 7G**). Still the average

395 number of remaining NeuN+ iNs per section was 50% lower in AAV9-miR-124 (58 ± 22 at 8w
396 *vs* 118 ± 42 at 3w p.i.) and 30% lower in miR-124+ISX9 (107 ± 12 at 8w *vs* 151 ± 25 at 3wp.i.)
397 **(Fig 7H)**. Interestingly the average number of NeuN+ iNs in the AA9-miR-124+ISX9 group was
398 almost double as compared to the AAV9-miR-124 group (107 ± 12 for AAV9-miR-124+ISX9
399 *vs*58 ± 22 for AAV9-miR-124) **(Fig 7H),** indicating that ISX9 enhances the survival of converted
400 iNs. However, the majority of reprogrammed iNs in both conditions retained an immature
401 neuronal morphology even at the time point of 8wp.i. (**Suppl Fig 8C and Suppl Fig 9F and G**).
402 Of note, mCherry expression was also observed in several resident pyramidal neurons mostly
403 in the broader peritraumatic region at both time points, a phenomenon very recently pointed
404 out for AAVs (Wang et al. 2021), however mCherry+ resident pyramidal neurons were
405 excluded from our analysis as they were easily distinguished by their morphology (large conic
406 soma and large apical process) (**Suppl Fig 8D and Suppl Fig 9C**).

407 Further on, to validate that produced iNs are the result of a reprogramming process, we
408 administered BrdU for 4 consecutive days starting 2 days after the cortical trauma to label
409 proliferating reactive astrocytes of the peritraumatic area (**Fig 7I**). Analysis 7 dp.i. revealed
410 that nearly 1/3 of transduced astrocytes (29.5 ± 16.3%) had incorporated BrdU (**Fig 7J**), while
411 BrdU+ transduced cells were still present 3w p.i. in both conditions (34.5% ± 5.5% for AAV9-
412 miR-124 and 33.5% ± 12.7% for AAV9-miR-124+ISX9) (**Suppl Fig 8E**). Importantly, 3w p.i. iNs
413 originating from a proliferating state expressing the cortical marker Tbr1were present (**Fig 7M**
414 **and Suppl Fig 9D and E)** at a percentage of 40.8% ± 3.7% in AAV9-miR-124 and 37.2% ± 13.6%
415 in AAV9-miR-124+ISX9 cells (**Fig 7K**) and accounted for nearly 1/5 of all transduced cells'
416 population (**Fig 7L**). Of note, BrdU+/Tbr1+ transduced cells were still present at 8w p.i. (**Suppl**
417 **Fig 8F**).

418 These findings collectively indicate that a significant subpopulation of iNs originates from a
419 proliferating fraction of reactive astrocytes. They also show that miR-124 is sufficient to drive
420 on its own neurogenic reprogramming of reactive astrocytes to immature iNs which remain
421 viable within the injured cortex for a period of at least 8w, while ISX9 administration seems to
422 enhance the survival of converted iNs.

423

424 ## Discussion

425 In this study we attempted to isolate miR-124 mechanism of action from that of other
426 reprogramming co-factors and aimed at identifying novel miR-124 targets with important
427 contribution in the reprogramming process. We provide evidence that miR-124 drives the
428 trans-differentiation switch of cortical astrocytes to an immature iN phenotype of cortical
429 identity, directing astrocytes through a multipolar intermediate stage expressing neurogenic
430 TFs associated with neuronal commitment and differentiation during embryonic (Kwan,
431 Šestan, and Anton 2012; Elsen et al. 2018) and adult neurogenesis (Díaz-Guerra et al. 2013).
432 In order to overcome the unexpected finding that miR-124 over-expression significantly
433 down-regulates the neuronal differentiation TF NeuroD1 (Z. Gao et al. 2009), we
434 supplemented miR-124 with the neurogenic compound ISX9, known to up-regulate neuronal
435 specific genes, among which NeuroD1. ISX9 acts by increasing intracellular Ca^{2+} signaling
436 leading to HDAC5 nuclear exit and MEF2 de-repression (Schneider et al. 2008) and has been
437 already used in chemical reprogramming protocols for the conversion of fibroblasts and
438 astrocytes to iNs (L. Gao et al. 2017; Li et al. 2015). Indeed, the addition of ISX9 greatly
439 improved both the reprogramming efficiency and differentiation status of miR-124+ISX9-iNs
440 *in vitro*, leading to the acquisition of electrophysiologically active iNs. Interestingly, despite
441 up-regulation of NeuroD1 levels and many other neuronal TFs by ISX9 alone, control sc-
442 miRNA+ISX9-treated astrocytes failed to undergo reprogramming. NeuroD1 has been
443 extensively reported to possess a strong 'pioneer factor' reprogramming capacity towards the
444 neuronal fate upon its viral-mediated overexpression (Pataskar et al. 2016; Matsuda et al.
445 2019), however very high levels of NeuroD1–not triggered by ISX9 supplementation in our
446 system– seem to be required to inflict these effects.

447 The RNA-Seq analysis we performed, highlighted the importance of miR-124 over-expression
448 in the down-regulation of astrocytic TFs, RBPs, EFs and components of signaling pathways with
449 significant regulatory role in astrocytic identity and function, which is in accordance with its
450 documented role in favoring neuronal fate at the expense of astrocytic (Neo et al. 2014) and
451 implies that astrocytic identity barriers need to be repressed before the induction of a
452 neuronal cell fate during the reprogramming process. Conversely, ISX9 had a small
453 contribution in the repression of astrocytic genes, thus this might be the reason for its inability
454 to confer the reprogramming switch on its own.

455 Our analysis of the direct miR-124 targets utilizing AGO-HITS-CLIP data from mouse cortex(Chi
456 et al. 2009) revealed the RBP *Zfp36l1* as a novel target of miR-124. Of note, we also verified

457 the miR-124/Zfp36l1 interaction in human bearing the same binding site, by analyzing AGO-
458 HITS-CLIP data from human motor cortex and cingulate gyrus (Boudreau et al. 2014), a finding
459 highlighting the importance of this conserved interaction during mammalian brain evolution.
460 Many studies have identified several direct targets of miR-124 with important regulatory role
461 in neurogenesis, acting at the transcriptional level, such as the TFs *Sox9* (Cheng et al. 2009),
462 *Lhx2* (Sanuki et al. 2011) and the components of the REST repressor complex, *Scp1*
463 (Visvanathan et al. 2007) and *Rcor1* (Baudet et al. 2012; Volvert et al. 2014); or at the
464 epigenetic level, such as the component of the PRC2 complex *Ezh2* (Neo et al. 2014) and the
465 component of the BAF complex *BAF53a* (Yoo et al. 2009); as well as at the post-transcriptional
466 level, such as the RBP involved in alternative splicing *Ptbp1*(Makeyev et al. 2007).

467 Here, we report for the first time that miR-124 is directly implicated in the regulation of
468 another process mediated by RBPs, the mRNA decay, apart from the well-characterized miR-
469 124/Ptbp1 circuitry (Yeom et al. 2018; Xue et al. 2013; Makeyev et al. 2007). Zfp36l1 is a
470 member of the Zfp36 family of proteins along with Zfp36 and Zfp36l2, which act by binding to
471 AU rich elements (AREs) in the 3'UTR of their mRNA targets mediating their destabilization
472 (Lai et al. 2000). Zfp36l1 is expressed in cortical radial glial precursors of the VZ (DeBoer et al.
473 2013; Yuzwa et al. 2017; Weng et al. 2019), cortical glial cells (Weng et al. 2019) and non-
474 neuronal cells (M. T. Chen et al. 2015; Carrick and Blackshear 2007). Interestingly, the ARE-
475 dependent mRNA decay is regulated by other neurogenic miRNAs as well, since the close
476 paralog of Zfp36l1, Zfp36, is targeted by miR-9 (Dai et al. 2015), suggesting a combined
477 regulation of Zfp36 family members by the two miRNAs to increase the stabilization of
478 neuronal mRNAs during neurogenesis.

479 In order to identify targets of Zfp36l1 being up-regulated in our system we examined data
480 from Zfp36l1-iCLIP-Seq experiments in thymocytes (Vogel et al. 2016) and B lymphocytes
481 (Galloway et al. 2016). Although our analysis was restricted to a non astrocytic transcriptome,
482 we identified a rather large number of Zfp36l1 targets being up-regulated in miR-124-iNs that
483 interestingly correspond to nearly half of the up-regulated genes by miR-124. Importantly,
484 many Zfp36l1 targets exhibit significant regulatory role in neurogenesis and neuronal
485 differentiation, such as the studied here TFs *Tox* and *Rcor2* and the RBPs *Rbfox1*, *Elavl4* and
486 *Nova1*. Having verified that Zfp36l1, and not Zfp36l2, is a direct target of miR-124, we used a
487 target site blocker (TSB) that efficiently antagonizes the binding of miR-124 in the 3'UTR of
488 *Zfp36l1* mRNA, to investigate whether Zfp36l1 targeting by miR-124 contributes to the cell
489 fate switch of astrocytes. Indeed the disruption of miR-124/Zfp36l1 interaction had a negative
490 impact on the reprogramming process, reducing the number of Tuj1+ miR-124-iNs and

491 abolishing their multipolar morphology. Of note, among the neuron-specific RBPs identified
492 as down-stream targets of Zfp36l1, *Rbfox1* and *Nova1* exhibit a pattern of direct post-
493 transcriptional regulation in contrast to *Elavl4*, implying the stronger involvement of other
494 RBPs in its post-transcriptional regulation. In accordance with this, Zfp36 has been reported
495 to target *Elavl2, Elavl3, Elavl4* and *Nova1* (Dai et al. 2015), uncovering a complementary and
496 synergistic role of Zfp36l1 and Zfp36in repressing neuron-specific RBPs in non-neuronal cells.

497 Furthermore, the addition of ISX9 significantly contributed to the robust up-regulation of the
498 mRNA levels of *Rbfox1*, *Elavl2, Elavl4* and most prominently Elavl3, reinforcing the action of
499 miR-124 in inducing the switch from the neuronal transcripts' destabilizing RBPs to the
500 stabilizing neuronal RBPs (Ince-Dunn et al. 2012; Weyn-Vanhentenryck et al. 2014, Scheckel
501 et al. 2016) through a different mechanism that would be interesting to be explored (**Fig 6H**).
502 Interestingly, miR-124 has been recently shown to synergize with Elavl3 for the enhancement
503 of target gene expression during neuronal maturation (Lu et al. 2021), further supporting our
504 observations for the role of ISX9 in promoting iNs' maturation in cooperation with miR-124.
505 In parallel, ISX9 supplementation greatly enhanced the transcriptional levels and the number
506 of TFs related to telencephalon development and/or adult neurogenesis, further promoting
507 the cortical identity of iNs already initiated by miR-124. Surprisingly, ISX9 also up-regulated a
508 large set of TFs related to the development of other non-telencephalic brain regions such as
509 the midbrain and the hindbrain/spinal cord. Of note, ISX9 has been shown to affect the
510 epigenetic landscape leading to an open chromatin state by increasing H3/H4 acetylation in
511 pancreatic β-cells (Dioum et al. 2011), suggesting that an epigenetic mechanism may be
512 responsible for the observed transcriptional regional expansion, a hypothesis that needs to
513 be further explored.

514 Here we also explored the *in vivo* capacity of miR-124 to induce direct neurogenic
515 reprogramming of astrocytes in a mouse cortical injury model, known to render astrocytes
516 more plastic by activating NSC genes' expression, thus facilitating their reprogramming (Götz
517 et al. 2015). *In vivo* reprogramming of reactive astrocytes to neuronal precursors and iNs has
518 been achieved following forced expression of TFs among which Sox2 (Niu et al. 2013), Neurog2
519 (Grande et al. 2013), NeuroD1 (Rivetti Di Val Cervo et al. 2017; Guo et al. 2014) and
520 Nurr1/Neurog2 (Mattugini et al. 2019), in some cases combined with anti-apoptotic and/or
521 anti-oxidant treatment to enhance survival (Gascón et al. 2016), however the *in vivo*
522 neurogenic capacity of miR-124 on its own has not been evaluated up to now. For this, we
523 employed two different viral-based approaches, using either lentiviruses or the more recently
524 used AAVs and corroborated the latter approach with BrdU administration during the peak

525 period of trauma-induced astrogliosis. The last years, the functional restoration of disease-
526 related symptoms upon direct reprogramming has been reported (Giehrl-Schwab et al. 2022;
527 Qian et al. 2020; Zhou et al. 2020; Z. Wu et al. 2020; Y. C. Chen et al. 2019), supporting the
528 therapeutic promise of *in vivo* direct reprogramming to restore impaired neuronal circuits
529 (Bocchi, Masserdotti, and Götz 2022). However, certain AAV-based strategies and astrocyte-
530 lineage tracing approaches have been very recently put under question as to their capacity to
531 confer neurogenic reprogramming (Wang et al. 2021). In light of this new challenge in the field
532 of *in vivo* reprogramming, we report here that both viral approaches point towards a
533 reprogramming capacity of miR-124 in converting reactive astrocytes of the peritraumatic
534 cortical area to iNs of cortical identity. More importantly, our AAV-based protocol combined
535 with BrdU administration, which is one of the very few widely accepted tools currently
536 available to verify the non-neuronal origin of reprogrammed cells, showed that about 1/3 of
537 iNs originated from proliferating astrocytes, strongly supporting the reprogramming potential
538 of miR-124 towards NeuN+/Tbr1+ iNs – harboring however an immature phenotype – that
539 persist in the peritraumatic area 8w following miR-124 over-expression. Additionally, our
540 analysis revealed that ISX9 supplementation seems to confer a survival advantage to the
541 converted iNs, implying a cell- or non-cell autonomous contribution of ISX9 in iNs' survival that
542 needs further exploration.

543 These findings indicate that, similarly to the *in vitro* situation, miR-124 is capable of inducing
544 the reprogramming switch of peritraumatic reactive astrocytes, but is not sufficient to further
545 enhance the maturation of produced immature iNs. Additionally, ISX9 *in vivo* administration
546 acts beneficially to reprogramming, by contributing majorly to iNs' enhanced survival for a
547 longer period, but in contrast to our *in vitro* observations it does not seem to reinforce iNs'
548 maturation, although that it is well accepted that it crosses the blood brain barrier in the
549 scheme that we administered it (Bettio et al. 2016). Further analysis of miR-124-iNs' and miR-
550 124+ISX9-iNs' molecular profiling using single cell RNA-Seq could shed light on the exact
551 differentiation state of miR-124-iNs and the possible enhancement of miR-124+ISX9-iNs'
552 maturation status by ISX9.

553

554 ## Ideas and speculation

555 Taken together this study highlights the strong potency of miR-124 to instruct the cell fate
556 switch of astrocytes, post-transcriptionally triggering cortical neurogenesis pathways being
557 unlocked in part by the direct targeting of *Zfp36l1*. Additionally, our *in vitro* results give
558 mechanistic insight into the combined action of miR-124 and ISX9 in driving direct
559 reprogramming of astrocytes to mature iNs. Importantly, our findings point to the *in vivo*
560 capacity of miR-124 to induce reactive astrocytes' reprogramming to immature iNs able to
561 survive for long periods, in particular following ISX9 supplementation, further supporting miR-
562 124 ' master reprogramming' potential. However, the synergistic effect of miR-124/ISX9 does
563 not seem to be sufficient to drive iNs' full maturation, indicating that more intrinsic and/or
564 extrinsic cues are required. To this end the findings of our *in vitro* mechanistic studies point
565 to certain common transcriptional and post-transcriptional downstream effectors of miR-124
566 and ISX9 that are known to promote neurogenesis and neuronal differentiation and thus bear
567 the potential to amplify miR-124/ISX9 combined *in vivo* reprogramming capacity and to
568 enhance the differentiation/ maturation of newly produced iNs. This strategy comes in
569 accordance with a very recent view in the reprogramming field arguing that *in vivo* glia-to-
570 neuron conversion is a two-stage process involving initial immature iNs production and their
571 subsequent differentiation provided that certain still largely unknown barriers are over-
572 passed (Leaman, Marichal, and Berninger 2022). Thus focusing on the points of convergence
573 of miR-124/ISX9 action holds promise for the establishment of a more efficient, *in vivo*
574 reprogramming protocol to improve maturation of iNs and their functional integration in the
575 host circuit following trauma or neurodegeneration.

576 # Materials and Methods

577 **Primary cultures of postnatal cortical astrocytes**

578 Primary postnatal astrocytic cultures from P3-P5 mice were prepared as previously
579 described(Aravantinou-Fatorou et al. 2015). Briefly, the cerebral cortexes from 2-3 P3-P5
580 C57BL/6 mice were collected in ice cold HBSS (Invitrogen), the tissue was washed three times
581 with HBSS and digested with 0.04% trypsin (Sigma) and 10μg/ml DNAse (Sigma) for 5 min at
582 37°C. After digestion cells were mechanically dissociated, centrifuged for 5 min at 850 rpm
583 (120 g), re-suspended in DMEM 4.5g/lt glucose (Invitrogen) containing 10% FBS (Invitrogen),
584 1% Penicillin/Streptomycin (Pen/Strep) (Sigma) and placed in a T75 flask pre-coated with poly-
585 D-lysine (PDL) (Sigma). When culture reached confluence (usually after 7 days), the flask was
586 shaken in a horizontal shaker at 200-250 rpm for 20h, in order to obtain a pure astrocytic
587 culture, free from neurons, oligodendrocytes and microglia. The remaining cells were digested
588 with 0.5% trypsin-EDTA (Invitrogen) for 5 min at 37°C, centrifuged at 850 rpm, re-suspended
589 in fresh DMEM 4.5g/lt glucose 10% FBS, 1% Pen/Strep and divided in two new T75 flasks pre-
590 coated with PDL. Half of the medium was changed every two days.

591 **In vitro reprogramming protocol**

592 For the reprogramming of astrocytes to induced-neurons, 40,000 astrocytes were seeded in
593 10mm coverslips coated with 20μg/ml poly-L-ornithine (PLO) (Sigma) overnight and 5μg/ml
594 laminin for 3h at 37°C (Sigma). Once cells reached>90% confluence (usually after 1-2 days)
595 they became transfected with 80nM miR-124-3p mimics or scrambled (sc-miRNA) mimics
596 (negative control) (Thermo) using Lipofectamine 2000 (Invitrogen) according to
597 manufacturer's instructions (d1). The next day the astrocytic medium (DMEM 4.5g/lt glucose,
598 10% FBS, 1% Pen/Strep) was replaced with the reprogramming medium: Neurobasal
599 (Invitrogen) supplemented with 1X B-27 (Invitrogen), 1X GlutaMAX (Invitrogen), 20μM vitamin
600 E (a-tocopherol) (Sigma) and 200mM ascorbic acid (Sigma). The same process of transfection
601 was repeated twice at d3 and d5. Vitamin E was added to the medium until d4, while ascorbic
602 acid was added throughout the reprogramming protocol. At d7 the reprogramming medium
603 was changed to the neuronal differentiation medium: Neurobasal supplemented with 1X B-
604 27, 1X GlutaMAX, 20ng/ml BDNF (R&D Systems), 0.5mM cAMP (Sigma) and 200mM ascorbic
605 acid. In the miR-124+ISX9-reprogrammed cells, 10μM of ISX9 chemical compound (Tocris)
606 were added from d2 to d10. All the mediums added to the reprogrammed cells were pre-
607 conditioned for 24h in a confluent astrocytic culture.

608 For BrdU administration, astrocytes were treated with 10μM BrdU (Sigma) two times per day
609 from day1 until day4 of the reprogramming protocol and analyzed at d7.

610 **RT-qPCR analysis**

611 For the RT-qPCR analysis experiments, total RNA was extracted using the Nucleospin miRNA
612 kit (Macherey-Nagel) and 500-800ng of total RNA were used for cDNA synthesis with the
613 Superscript II reverse transcriptase (Invitrogen) according to manufacturer's instructions.
614 Quantitative real time PCR was performed using SYBR Select Master Mix (Applied Biosystems)
615 and samples were run in the ViiA 7 Real-Time PCR System (Applied Biosystems). The primers
616 used are listed in **Table 1**. Each sample was analyzed in triplicates, gene expression was
617 calculated using the ΔΔCt method and all the results were normalized to β-actin expression.
618 Relative expression was estimated setting the values of sc-miRNA transfected astrocytes to 1.
619 All experiments were performed at least in triplicates.

620 **Immunocytochemistry**

621 Cells were washed once with PBS and then fixed with 4% paraformaldehyde for 20 min at
622 room temperature. Afterwards, cells were washed three times with PBS and blocked with 5%
623 normal donkey serum (NDS) (Merck-Millipore), 0.1% Triton X-100 in PBS for 1 h at room
624 temperature. For nuclear staining, cells were permeabilized with 0.25% Triton X-100 in PBS
625 for 10 min at room temperature and washed three times with PBS prior to blocking. For BrdU
626 staining cells were incubated with 2M HCl, 0.1% Triton X-100 at 37°C for 10 min and then with
627 0.1M Sodium Borate (pH:8.5) for 30 min at room temperature followed by washing three
628 times with PBS prior to blocking. Next, cells were incubated with primary antibodies, diluted
629 in 1% NDS, 0.05% Triton X-100 in PBS overnight at 4°C. The next day, cells were washed three
630 times with PBS and incubated with secondary antibodies diluted in 1% NDS, 0.05% Triton X-
631 100 in PBS for 2h at room temperature. The nuclei of the cells were stained with ProLong Gold
632 Antifade Reagent with DAPI (Cell Signaling). The following primary antibodies were used in
633 this study: rabbit anti-GFAP (DAKO, 1:600), mouse anti-GFAP (Cell Signaling, 1:600), mouse
634 anti-Tuj1 (Covance, 1:600), chicken anti-Tuj1 (Millipore, 1:1000), rabbit anti-Iba1 (WAKO,
635 1:400), rabbit anti-PDGFRa (Cell Signaling, 1:1000), mouse anti-NG2 (Millipore, 1:500), rat
636 anti-BrdU (Oxford Biotech, 1:50), mouse anti-MAP2 (Millipore, 1:200), rabbit anti-Synapsin1
637 (Abcam, 1:200), rat anti-Mash1 (R&D Systems, 1:100), rabbit anti-Tbr2 (Abcam, 1:200), rabbit
638 anti-Gsx2 (Millipore, 1:400), rabbit anti-Tox (Atlas antibodies, 1:200), mouse anti-vGlut1
639 (Millipore, 1:1000) and rabbit anti-GABA (Sigma, 1:10,000). The secondary antibodies used in
640 this study were Alexa Fluor 546-, Alexa Fluor 488- and Alexa Fluor 647-conjugated secondary

641 antibodies (Life Technologies). Images were acquired with a 20x or 40x objective (1024x1024
642 pixels, 1µm Z-step) using a Leica TCS SP8 confocal microscope (LEICA Microsystems). For each
643 experiment measurements from 20-25 fields per coverslip were obtained for each condition.

644 **Electrophysiology**

645 For whole-cell recordings iNs plated in PLO-laminin coated coverslips were used for
646 electrophysiological experiments beginning at d15 up to d27 of the reprogramming protocol.
647 The coverslips with the cells were placed onto a recording chamber and viewed using an
648 Olympus CKX41 microscope with a 40x lens. The cells were bathed in a solution containing:
649 140mM NaCl, 2.8mMKCl, 2mM $CaCl_2$, 4mM $MgCl_2$, 10mM Glucose, and 20mM HEPES. For
650 whole-cell recordings we used a capillary glass with Filament (Sutter instrument) to fabricate
651 low resistance recording pipettes (~5 MΩ) and filled with: 140mMKCl, 2mM $CaCl_2$, 2mM
652 $MgCl_2$, 2mM Mg-ATP, 5mM EGTA and 10mMHEPES. Osmolarity and pH of all solutions were
653 adjusted appropriately before experiments. Data were acquired at room temperature (22–
654 24°C) using an EPC9 HEKA amplifier and an ITC-16 acquisition system with a patch master
655 software (HEKA). Data analysis was carried out using OriginPro8. **Voltage protocols:** The
656 membrane of the cells was held at a holding potential of -70 mV and step depolarizing pulses
657 were applied. Depolarization steps were applied for 50 msec in 10 mV increments from -80
658 mV to +50 mV with a sweep interval time of 1 sec and sweep duration of 500 ms.Each
659 depolarizing pulse was proceeded by a hyperpolarizing step to -120 mV. **Current protocols:**
660 Cells we held at their resting membrane potential (0pA) and depolarizing current steps from -
661 20 pA to 200 pA from a holding current of 0pA were applied.

662 **RNA-Seq experiment and Bioinformatics analysis**

663 For the RNA-Seq experiment, the following samples were prepared in 3 biological replicates:
664 astrocytes (d1), sc-miRNA-transfected astrocytes (d7), miR-124-iNs (d7) and miR-124+ISX9-iNs
665 (d7). Total RNA was extracted using the Nucleospin miRNA kit (Macherey-Nagel) according to
666 manufacturer's instructions. Libraries were prepared with TruSeq RNA Library Prep Kit v2
667 (Illumina) and 75c single-end sequencing in an Illumina NextSeq 550 sequencer. Raw libraries
668 were quality checked and preprocessed using Fast QC
669 (https://www.bioinformatics.babraham.ac.uk/projects/fastqc/). Mapping of reads against
670 the Mouse Transcriptome (v.GRCm38.rel79) and transcript abundance estimation on
671 Transcripts Per Million (TPM) values was performed using kallisto (Bray et al. 2016). Analysis
672 of differential expression, interpretation and visualization was subsequently performed using
673 kallisto-compatible Sleuth tool (Pimentel et al. 2017) and R-base functions. Gene ontology

674 (GO) enrichment analysis was performed using the Gene Ontology Panther Classification
675 System (http://pantherdb.org/).

676 **Analysis of AGO-CLIP-Seq data**

677 AGO-HITS-CLIP datasets, performed in mouse brain cortex tissue (P13 neocortex, 5 replicates)
678 and human brain tissues (motor cortex, cingulate gyrus) from 2 individuals, were retrieved
679 from the publications (Chi et al. 2009) and (Boudreau et al. 2014) respectively. Raw libraries
680 were quality checked using FastQC (www.bioinformatics.babraham.ac.uk/projects/fastqc/),
681 while adapters/contaminants were detected utilizing an in-house developed pipeline and the
682 Kraken suite (Davis et al. 2013). Pre-processing was performed with Trim Galore (Krueger
683 2015) and Cutadapt (Martin 2011). CLIP-Seq libraries were aligned against the reference
684 genomes, i.e. GRCh38 and mm10 assemblies for human and mouse respectively, with
685 GMAP/GSNAP (T. D. Wu and Nacu 2010) spliced aligner, allowing up to 2 mismatches.
686 microCLIP CLIP-Seq-guided model (Paraskevopoulou et al. 2018) was utilized to identify
687 binding events for the expressed miRNAs. In case of multiple replicates (i.e. mouse brain
688 cortex) a miRNA binding event had to be present in at least two replicates to be considered
689 as valid. Top expressed miRNAs were retrieved from the relevant publications. Human and
690 mouse transcriptomes were compiled from ENSEMBL v96 (Cunningham et al. 2019) to
691 annotate the retrieved miRNA binding events. Identified miRNA binding sites residing on 3'
692 UTR regions were retained and subsequently filtered to preserve only genes expressed in
693 astrocytes. A list of ~10,000 genes, expressed in astrocytes, with FPKM≥2, was retrieved from
694 a reference publication and retained for analysis (Y. Zhang et al. 2014).

695 **3'-UTR cloning and measurement of Luciferase activity**

696 A cDNA fragment of 710 bp corresponding to the 3'-UTR of Zfp36l1, containing the 7-mer
697 binding site of mmu-miR-124-3p.1 (5'-TACAGAAGCAACTTGA**GTGCCTT**-3'), was obtained from
698 RNA that was isolated from astrocytes using oligo dT primer for cDNA synthesis and
699 subsequently the specific primers **Zfp36l1FOR**: 5'-ATC*GAGCTC*CACATAAGGACAAGTCAATTT
700 and **Zfp36l1REV**: 5'-TGC*TCTAGA*AGCTTTTCTCTCATTTGTTGTCA for PCR amplification. The PCR
701 fragment was subcloned into pmiR-GLO reporter vector (Promega) at the *SacI* and *XbaI*
702 restriction sites. In addition, a cDNA fragment of 860bp corresponding to the 3'UTR of Zfp36l2,
703 containing the two adjacent putative 7-mer binding sites of mmu-miR-124-3p.1 (5'-
704 GGGGAAATGGTCTCA**GTGCCTT**-3' and 5'-CATAGGGCCCGAACT**TGCCTTA**-3' respectively), was
705 amplified as previously using the specific primers **Zfp36l2FOR**: 5'-
706 ATC*GAGCTC*GTTCTTTTCACAGTAATATATGC-3' and **Zfp36l2REV**: 5'-

707 TG*CTCTAGA*CCAAAAAATTTTATTGGGGGAAAC-3' respectively. All PCR products were
708 subcloned into pmiR-GLO vector at the *SacI* and *XbaI* restriction sites and then were subjected
709 to sequencing. Mutation of the verified 7-mer binding site of the 3'-UTR of Zfp36l1 was
710 performed using the Q5-site directed mutagenesis kit (New England BioLabs) using the
711 following primers: **Zfp36L1mutFOR**: 5'-TTTGTAATCTAACTTTGTCACTG-3' and
712 **Zfp36L1mutREV**: 5'-AAAATAAGTTGCTTCTGTAAACG-3' and resulted in a mutated 7-mer
713 binding site 5'-TACAGAAGCAACTTGA**TTTTTTT**-3'. All mutated clones were subjected to
714 sequencing.

715 Luciferase assays were performed in HEK293T cells at 50-60% confluence. HEK293T cells were
716 co-transfected with the 3'UTR-containing pmiR-GLO reporter constructs (1 µg) along with sc-
717 miRNA or miR-124 mimics (80 nM, Thermo) using Lipofectamine 2000 (Thermo) and 48 h later
718 luciferase activity was measured in cell lysates using the Firefly & Renilla Single Tube
719 Luciferase Assay Kit (Biotium), according to manufacturer's instructions. Firefly luciferase
720 activity was normalized with Renilla luciferase activity measured in the same tube and the
721 normalized Firefly luciferase activity for cells transfected with sc-miRNA was set to 1, thus
722 estimating the fold change of normalized Firefly luciferase activity inflicted by miR-124
723 transfection for each construct.

724 **Target Site Blocker (TSB) experiment**

725 For the functional validation of the miR-124/Zfp36l1 interaction a custom made miRCURY
726 locked nucleic acid (LNA) miRNA Power Target Site Blocker (TSB) (Qiagen) was used with the
727 following sequence: TTACAAGGCACTAAGTTGCTT. TSB was transfected in astrocytes along
728 with sc-miRNA or miR-124-3p mimics using Lipofectamine 2000 (Invitrogen) in different
729 molecular ratios: miR-124:TSB, 4:1 (80nM:20nM), 2:1 (80nM:40nM) and 1:1 (80nM:80nM).

730 **Western blot**

731 Cells were washed once with ice-cold PBS and lysed for 15min in ice-cold lysis buffer (150mM
732 NaCl, 50mM Tris (pH 7.5), 1%v/v Triton X-100, 1mM EDTA, 1mM EGTA, 0.1% SDS, 0.5% sodium
733 deoxycholate) containing PhosSTOP phosphatase inhibitors and a complete protease inhibitor
734 mixture (Roche Life Science), then centrifuged at 20,000 g for 15min, followed by collection
735 of the supernatant and measurement of the protein concentration by Bradford assay
736 (Applichem). Proteins were separated by SDS-polyacrylamide gel electrophoresis (PAGE) and
737 transferred onto nitrocellulose membranes (Maine Manufacturing). Nonspecific binding sites
738 were blocked in TBS, 0.1% Tween 20, 5% skimmed milk for 1 h at room temperature followed
739 by overnight incubation with primary antibodies diluted in TBS, 0.1% Tween20, 5% BSA.

740 Primary antibodies used were rabbit anti-Zfp36l1/Zfp36l2 (this antibody recognizes Zfp36l1 at
741 37kDa and Zfp36l2 at 51kDa) (Abcam, 1:500) and mouse anti-βactin (Millipore, 1:1000).
742 Incubation with HRP-conjugated secondary antibodies, anti-mouse-HRP (Thermo, 1:10,000)
743 and anti-rabbit-HRP (Thermo, 1:5,000) was performed for 2 h at room temperature and
744 protein bands were visualized using the Clarity Western ECL Substrate (BIO-RAD).

745 **Lentiviral production**

746 For lentiviral *in vivo* transduction, VSV-G (Vesicular Stomatitis Virus–Glycoprotein)–
747 pseudotyped lentiviruses were used either for the over-expression of miR-124 along with GFP
748 or as control expressing only GFP. More specifically, for lentiviral particles' production, HEK
749 293T cells cultured in 10-cm Petri dishes at a 50-60% confluence were co-transfected with 10
750 µg lentiviral plasmid expressing miR-124-1 precursor under the CMV promoter and GFP under
751 the EF1 promoter (SBI System Biosciences) or 10 µg lentiviral plasmid expressing GFP under
752 the CMV promoter and the packaging plasmids pVSV-G (3.5 µg), MDL (6.5 µg), and RSV-REV
753 (2.5 µg) (all kindly provided by Dr. Matsas' lab) with calcium phosphate. The following day the
754 culture medium was replaced with fresh one, the supernatant containing the lentiviral
755 particles was collected 48 h and 72 h (second harvest) after transfection and concentrated by
756 ultracentrifugation at 25,000 rpm (80,000 x g) for 2 h at 4°C using a sucrose gradient.

757 ***In vivo* reprogramming protocols**

758 This study was carried out in strict compliance with the European Directive 2010/63/EU and
759 the Greek National Law 161/91 for Use of Laboratory Animals, according to FELASA
760 recommendations for euthanasia and the National Institutes of Health Guide for Care and Use
761 of Laboratory Animals. All protocols were approved by the Animal Care and Use Committee
762 of the Hellenic Pasteur Institute (Animal House Establishment Code: EL 25 BIO 013). License
763 No 2585/31-5-18 and 490073/15-6-21 for the experiments was issued by the Greek
764 authorities of the Veterinary Department of the Athens Prefecture. The manuscript was
765 prepared in compliance with the ARRIVE guidelines for reporting animal research.
766

767 **Cortical Trauma model:** Adult male and female FVB or Rosa26-EYFP reporter mice (8-16 weeks
768 old) were deeply anaesthetized using inhalable isoflurane, and positioned in a stereotaxic
769 apparatus. The dorsal surface of the skull was exposed through a midline incision and a burr
770 hole was drilled at the following coordinates: antero-posterior (AP) -1.0 mm, caudal to
771 Bregma; lateral (L) 1.0 mm to the midline. A 26-gauge needle was inserted into the brain
772 parenchyma in a depth of 0.9 mm from the surface of the brain to create a trauma in the
773 cortex, avoiding the corpus callosum and hippocampus. The inserted needle was moved along

774 the anterior-posterior axis between positions (AP) -1.1 and -0.9 to widen the trauma. The skin
775 was sutured, a local analgesic cream containing 2.5% lidocain and 2.5% prilocain was applied
776 and the animals were kept warm until they were fully awake. Viral injection took place 4 days
777 after the cortical trauma.
778 **Lentiviral injection in the cortex of FVB mice:** A 10µl Hamilton syringe (Hamilton) with a 26-
779 gauge needle was slowly inserted into the brain tissue at coordinates (AP) -1.1 mm, (L) 1.0
780 mm, and (V): 1.0 mm, from the same burr hole on the skull and 2µl of lentiviral concentrate
781 was injected at a rate of 0.5 µl/min. The needle was left in position for 5 min after each
782 injection and then withdrawn gently. A second viral injection was repeated at coordinates (AP)
783 -0.9 mm, (L) 1.0 mm, and (V): 1.0 mm with similar procedures, and surgery was completed as
784 described above. A group of animals was injected with the lentivirus LV-miR-124-GFP and
785 another one with the control lentivirus LV-GFP. A subgroup of the LV-124 group received
786 intraperitoneally 20 mg/kg of ISX9 (Tocris) diluted in (2-Hydroxypropyl)-β-cyclodextrin (Sigma)
787 (ISX9 concentration: 2 mg/ml in 30% (2-Hydroxypropyl)-β-cyclodextrin (Sigma) diluted in
788 sterile ddH_2O) (Petrik et al. 2012; Kutsche et al. 2018) once a day, for 5 consecutive days,
789 beginning 48 h p.i. Animals were sacrificed 7 days or 3 weeks after viral injection.

790 **AAV injection in the cortex of R26R-EYFP mice:** 1,5µl of a viral mix (1:1) of AAV9:CMV-miR-
791 124-mCherry (titer: $\geq 5x10^{12}$ GC/ml, GeneCopoeia) and AAV5:GFAP-Cre (titer:$\geq 7\times10^{12}$ GC/ml,
792 Addgene) viruses were injected with a 10µl Neuros syringe (Hamilton) with a 33-gauge blunt
793 needle, at a rate of 0.25 µl/min, as described above. One subgroup in each time point (d7, 3w
794 and 8w) received i.p. 20 mg/kg of ISX9 as described above. BrdU (Sigma) (50mg/kg) was
795 administered twice a day, beginning at d2 after trauma for 4 consecutive days.

796 **Tissue Preparation, Histology, and Immunohistochemistry**

797 For histology, mice were deeply anaesthetized by inhaling isoflurane, and perfused with 4%
798 paraformaldehyde (PFA) via left cardiac ventricle. The brains were removed, post-fixed in 4%
799 PFA overnight and then cryo-protected in 20% sucrose overnight. Tissues were then frozen in
800 -20°C isopentane and cut into 20 µm-thick coronal sections on a cryostat (Leica CM1900),
801 collected on silane-coated slides and stored at -20°C. For detection of specific antigens with
802 immunofluorescence, sections were left for 15 min in room temperature, washed in PBS, and
803 blocked with 5% normal goat or donkey serum (Merck-Millipore) in PBS-T (0.1% Triton X-100
804 in PBS) for 1 h. Incubation with primary antibodies took place overnight at 4°C. Primary
805 antibodies used were: chicken polyclonal anti-GFP (Abcam, 1:1000), mouse monoclonal anti-
806 neuronal nuclei (NeuN) (Merck-Millipore, 1:300), rabbit polyclonal anti-glial fibrillary acidic

807 protein (GFAP) (Dako,1:600), mouse monoclonal anti-GFAP (Cell Signaling, 1:600); rabbit
808 polyclonal anti-oligodendrocyte transcription factor 2 (Olig2) (Merck-Millipore, 1:200), rabbit
809 polyclonal anti-ionized calcium-binding adapter 1 (Iba-1) (Wako, 1:600) rabbit polyclonal anti-
810 Tbr1 (Abcam,1:250), rat monoclonal anti-BrdU (Oxford Biotech, 1:100), rat monoclonal anti-
811 red fluorescent protein (RFP) (Chromotek, 1:1000) and goat anti-mCherry (1:1000). Following
812 incubation with primary antibodies, sections were washed with PBS and incubated for 2 h with
813 the appropriate secondary antibodies conjugated with Alexa Fluor 488 (green), 546 (red), or
814 647 (blue). For nuclei staining sections were incubated with Hoechst (Molecular Probes) and
815 coverslipped with Mowiol (Calbiochem) or with DAPI using the Everbrite mounting medium
816 with DAPI (Biotium). Images were acquired with a 40x objective using Leica TCS SP8 and Leica
817 TCS-SP5II confocal microscopes (LEICA Microsystems).

818 **Image analysis**

819 Images were analyzed using Fiji/ImageJ software (National Institutes of Health) and Imaris
820 Software (Bitplane).
821 **In vitro analysis:** mean fluorescence intensity of Tbr2, Tox and Mash1 staining inside the cell
822 nuclei was quantified using a custom-written macro implemented in Fiji. Initially automatic
823 detection of nuclei was performed using the Otsu method and Tuj1+cells were selected based
824 on their mean intensity value above a user-defined threshold of 40, followed by a manual
825 validation according to cell morphology (cells with an astrocyte-like morphology with a big,
826 rectangular soma and none or few processes were excluded). Mean fluorescence intensity of
827 Tbr2, Tox and Mash1 inside the cell nuclei ROIs was measured both forTuj1- and Tuj1+ cells.
828 Quantification was performed in maximum intensity projections. For each experiment
829 measurements from at least 200-300 cells were obtained for each condition.
830 Morphological characterization of Tuj1+ cells in the TSB blocker experiments was also
831 conducted using Fiji. More specifically, morphological characterization included quantification
832 of the cell body area and the number of processes extending from the soma of Tuj1+ cells.
833 Tuj1+ cells were selected based on the mean intensity value of their soma above a user-
834 defined threshold and were sorted in 3 groups: cells with a multipolar morphology bearing 3
835 or more processes extending from the soma, cells with 1-2 processes and cells exhibiting an
836 astrocyte-like morphology with a rectangular soma possessing none or 1-2 processes.
837 Quantification was performed in maximum intensity projections. For each experiment
838 measurements from at least 100-150 cells were obtained for each condition.
839 **In vivo analysis:** for each animal and each immunofluorescence staining, cell counting was
840 performed on brain coronal sections collected at 240 mm intervals across the whole antero-

841 posterior extent of the hippocampus (Bregma -0.5mm up to -2.5mm) in a total number of 3-4
842 mice for each experimental condition. For estimation of the percentage of LV or AAV
843 transduced cells that have a specific phenotype, images of GFP+ or mCherry+ cells respectively
844 found in each set of sections were acquired and double- or triple-positivity with cell type-
845 specific markers was evaluated. All GFP+ or mCherry+ cells found in the cortex within these
846 sections were imaged and analyzed. For the analysis of AAV9-transduced cells mCherry+
847 mature neurons were excluded from the analysis. To isolate and evaluate morphological
848 features of astrocytes, resident neurons and iNs we used Imaris Contour Surface and Surface
849 Segmentation (Imaris v.9.3.1, Bitplane) for each channel represented in **Suppl Fig. 9**. Same
850 threshold values were used for all groups during the analysis.

851 **Statistical analysis**

852 All *in vitro* quantified data are presented as average ± SD, unless otherwise indicated. Two-
853 tailed Student t-test was used to calculate statistical significance with p values for all the data
854 obtained from the experiments with the TSB blocker, while for the rest of the data a one-
855 tailed Student t-test was used. p values less than 0.05 ($p<0.05$) were considered indicative of
856 significance. *In vivo* data were assessed using a one-way analysis of variance (ANOVA). When
857 interactions were detected, group comparisons were performed using a two-sample assuming
858 unequal variances test.

859

860 Acknowledgments

861 This work was financially supported by: 'BIOIMAGING-GR: A Greek Research Infrastructure for
862 Visualizing and Monitoring Fundamental Biological Processes (MIS 5002755)', funded by the
863 Operational Program "Competitiveness, Entrepreneurship and Innovation" (NSRF 2014-2020),
864 co-financed by Greece and the European Union (European Regional Development Fund);
865 ARISTEIA-II 'Astro-Rep' 3713 Excellence Grant of the Greek Ministry of Education and
866 Fondation Santé Grant 2017-2018, awarded to DT. We also acknowledge funding from the
867 Stavros Niarhos Foundation (SFN) Grant to the Hellenic Pasteur Institute, as part of the
868 Foundation's initiative to support the Greek Research Center Ecosystem; Greek General
869 Secretariat of Research and Technology 'Action for the Study of Neurodegenerative Diseases
870 on the Basis of Precision Medicine' and 'KRIPIS-II' Action (MIS 5002486) under the Operational
871 Strategic Reference Framework 2014–2020. We would like to thank Dr. Era Taoufik for critical
872 comments on the manuscript.

Author Contributions

EP and DT conceived whole project, designed experiments and analyzed the data; EP, CG, MG and MM conducted in vitro experiments; DCT and SJT designed and performed electrophysiology experiments; TK, DK and AGH designed and performed bioinformatics analysis and EP contributed in analyzing the data; PNK and IT designed and performed *in vivo* experiments, PKN and EP analyzed relevant data and PKN contributed in paper writing; EX developed the Fiji macro and helped with image analysis workflow; EP and DT wrote the manuscript; DT supervised the project and acquired funding.

Conflict of interest

The authors report no conflict of interest.

Data Availability

High throughput RNA-Sequencing data are deposited in the European Nucleotide Archive under Study accession PRJEB38603.

References

Abernathy, Daniel G., Woo Kyung Kim, Matthew J. McCoy, Allison M. Lake, Rebecca Ouwenga, Seong Won Lee, Xiaoyun Xing, et al. 2017. "MicroRNAs Induce a Permissive Chromatin Environment That Enables Neuronal Subtype-Specific Reprogramming of Adult Human Fibroblasts." *Cell Stem Cell* 21 (3): 332-348.e9. https://doi.org/10.1016/j.stem.2017.08.002.

Acaz-Fonseca, Estefania, Ana Ortiz-Rodriguez, Iñigo Azcoitia, Luis M. Garcia-Segura, and Maria Angeles Arevalo. 2019. "Notch Signaling in Astrocytes Mediates Their Morphological Response to an Inflammatory Challenge." *Cell Death Discovery*. https://doi.org/10.1038/s41420-019-0166-6.

Ambasudhan, Rajesh, Maria Talantova, Ronald Coleman, Xu Yuan, Saiyong Zhu, Stuart A. Lipton, and Sheng Ding. 2011. "Direct Reprogramming of Adult Human Fibroblasts to Functional Neurons under Defined Conditions." *Cell Stem Cell*. https://doi.org/10.1016/j.stem.2011.07.002.

Aravantinou-Fatorou, Katerina, Felipe Ortega, Dafni Chroni-Tzartou, Nasia Antoniou, Cornelia Poulopoulou, Panagiotis K. Politis, Benedikt Berninger, Rebecca Matsas, and Dimitra Thomaidou. 2015. "CEND1 and NEUROGENIN2 Reprogram Mouse Astrocytes and Embryonic Fibroblasts to Induced Neural Precursors and Differentiated Neurons." *Stem Cell Reports* 5 (3): 405–18. https://doi.org/10.1016/j.stemcr.2015.07.012.

Baudet, Marie Laure, Krishna H. Zivraj, Cei Abreu-Goodger, Alistair Muldal, Javier Armisen, Cherie Blenkiron, Leonard D. Goldstein, Eric A. Miska, and Christine E. Holt. 2012. "MiR-124 Acts through CoREST to Control Onset of Sema3A Sensitivity in Navigating Retinal Growth Cones." *Nature Neuroscience*. https://doi.org/10.1038/nn.2979.

Berninger, Benedikt, Marcos R. Costa, Ursula Koch, Timm Schroeder, Bernd Sutor, Benedikt Grothe, and Magdalena Götz. 2007. "Functional Properties of Neurons Derived from in Vitro Reprogrammed Postnatal Astroglia." *Journal of Neuroscience* 27 (32): 8654–64. https://doi.org/10.1523/JNEUROSCI.1615-07.2007.

Bettio, Luis E.B., Anna R. Patten, Joana Gil-Mohapel, Natasha F. O'Rourke, Ronan P. Hanley, Samantha Kennedy, Karthik Gopalakrishnan, Ana Lúcia S. Rodrigues, Jeremy Wulff, and Brian R. Christie. 2016. "ISX-9 Can Potentiate Cell Proliferation and Neuronal Commitment in the Rat Dentate Gyrus." *Neuroscience* 332: 212–22. https://doi.org/10.1016/j.neuroscience.2016.06.042.

Birtele, Marcella, Yogita Sharma, Srisaiyini Kidnapillai, Shong Lau, Thomas B. Stoker, Roger A. Barker, Daniella Rylander Ottosson, Janelle Drouin-Ouellet, and Malin Parmar. 2019. "Dual Modulation of Neuron-Specific MicroRNAs and the REST Complex Promotes Functional Maturation of Human Adult Induced Neurons." *FEBS Letters* 593 (23): 3370–80. https://doi.org/10.1002/1873-3468.13612.

Bocchi, Riccardo, Giacomo Masserdotti, and Magdalena Götz. 2022. "Direct Neuronal Reprogramming: Fast Forward from New Concepts toward Therapeutic Approaches." *Neuron* 110 (3): 366–93. https://doi.org/10.1016/j.neuron.2021.11.023.

Boudreau, Ryan L., Peng Jiang, Brian L. Gilmore, Ryan M. Spengler, Rebecca Tirabassi, Jay A. Nelson, Christopher A. Ross, Yi Xing, and Beverly L. Davidson. 2014. "Transcriptome-Wide Discovery of MicroRNA Binding Sites in Human Brain." *Neuron*. https://doi.org/10.1016/j.neuron.2013.10.062.

Bray, Nicolas L., Harold Pimentel, Páll Melsted, and Lior Pachter. 2016. "Near-Optimal Probabilistic RNA-Seq Quantification." *Nature Biotechnology*. https://doi.org/10.1038/nbt.3519.

Carrick, Danielle M., and Perry J. Blackshear. 2007. "Comparative Expression of Tristetraprolin (TTP) Family Member Transcripts in Normal Human Tissues and Cancer Cell Lines." *Archives of Biochemistry and Biophysics*. https://doi.org/10.1016/j.abb.2007.04.011.

Chen, Ming Tai, Lei Dong, Xin Hua Zhang, Xiao Lin Yin, Hong Mei Ning, Chao Shen, Rui Su, et al. 2015. "ZFP36L1 Promotes Monocyte/Macrophage Differentiation by Repressing CDK6." *Scientific Reports*. https://doi.org/10.1038/srep16229.

Chen, Yu Chen, Ning Xin Ma, Zi Fei Pei, Zheng Wu, Fabricio H. Do-Monte, Susan Keefe, Emma Yellin, et al. 2019. "A NeuroD1 AAV-Based Gene Therapy for Functional Brain Repair after Ischemic Injury through In Vivo Astrocyte-to-Neuron Conversion." *Molecular Therapy* 28 (1): 1–18. https://doi.org/10.1016/j.ymthe.2019.09.003.

Cheng, Li Chun, Erika Pastrana, Masoud Tavazoie, and Fiona Doetsch. 2009. "MiR-124 Regulates Adult Neurogenesis in the Subventricular Zone Stem Cell Niche." *Nature Neuroscience*.

https://doi.org/10.1038/nn.2294.
Chi, Sung Wook, Julie B. Zang, Aldo Mele, and Robert B. Darnell. 2009. "Argonaute HITS-CLIP Decodes MicroRNA-MRNA Interaction Maps." *Nature*. https://doi.org/10.1038/nature08170.
Cunningham, Fiona, Premanand Achuthan, Wasiu Akanni, James Allen, M. Ridwan Amode, Irina M. Armean, Ruth Bennett, et al. 2019. "Ensembl 2019." *Nucleic Acids Research*. https://doi.org/10.1093/nar/gky1113.
Dai, Weijun, Wencheng Li, Mainul Hoque, Zhuyun Li, Bin Tian, and Eugene V. Makeyev. 2015. "A Post-Transcriptional Mechanism Pacing Expression of Neural Genes with Precursor Cell Differentiation Status." *Nature Communications*. https://doi.org/10.1038/ncomms8576.
Davis, Matthew P.A., Stijn van Dongen, Cei Abreu-Goodger, Nenad Bartonicek, and Anton J. Enright. 2013. "Kraken: A Set of Tools for Quality Control and Analysis of High-Throughput Sequence Data." *Methods*. https://doi.org/10.1016/j.ymeth.2013.06.027.
DeBoer, E. M., M. L. Kraushar, R. P. Hart, and M. R. Rasin. 2013. "Post-Transcriptional Regulatory Elements and Spatiotemporal Specification of Neocortical Stem Cells and Projection Neurons." *Neuroscience*. https://doi.org/10.1016/j.neuroscience.2013.05.042.
Díaz-Guerra, Eva, Jaime Pignatelli, Vanesa Nieto-Estévez, and Carlos Vicario-Abejón. 2013. "Transcriptional Regulation of Olfactory Bulb Neurogenesis." *Anatomical Record*. https://doi.org/10.1002/ar.22733.
Dioum, Elhadji M., Jihan K. Osborne, Sean Goetsch, Jamie Russell, Jay W. Schneider, and Melanie H. Cobb. 2011. "A Small Molecule Differentiation Inducer Increases Insulin Production by Pancreatic β Cells." *Proceedings of the National Academy of Sciences of the United States of America*. https://doi.org/10.1073/pnas.1118526109.
Elsen, Gina E., Francesco Bedogni, Rebecca D. Hodge, Theo K. Bammler, James W. MacDonald, Susan Lindtner, John L.R. Rubenstein, and Robert F. Hevner. 2018. "The Epigenetic Factor Landscape of Developing Neocortex Is Regulated by Transcription Factors Pax6→ Tbr2→ Tbr1." *Frontiers in Neuroscience*. https://doi.org/10.3389/fnins.2018.00571.
Galloway, Alison, Alexander Saveliev, Sebastian Łukasiak, Daniel J. Hodson, Daniel Bolland, Kathryn Balmanno, Helena Ahlfors, et al. 2016. "RNA-Binding Proteins ZFP36L1 and ZFP36L2 Promote Cell Quiescence." *Science*. https://doi.org/10.1126/science.aad5978.
Gao, Longfei, Wuqiang Guan, Min Wang, Huihan Wang, Jiali Yu, Qing Liu, Binlong Qiu, et al. 2017. "Direct Generation of Human Neuronal Cells from Adult Astrocytes by Small Molecules." *Stem Cell Reports* 8 (3): 538–47. https://doi.org/10.1016/j.stemcr.2017.01.014.
Gao, Zhengliang, Kerstin Ure, Jessica L. Ables, Diane C. Lagace, Klaus Armin Nave, Sandra Goebbels, Amelia J. Eisch, and Jenny Hsieh. 2009. "Neurod1 Is Essential for the Survival and Maturation of Adult-Born Neurons." *Nature Neuroscience*. https://doi.org/10.1038/nn.2385.
Gascón, Sergio, Elisa Murenu, Giacomo Masserdotti, Felipe Ortega, Gianluca L. Russo, David Petrik, Aditi Deshpande, et al. 2016. "Identification and Successful Negotiation of a Metabolic Checkpoint in Direct Neuronal Reprogramming." *Cell Stem Cell* 18 (3): 396–409. https://doi.org/10.1016/j.stem.2015.12.003.
Giehrl-Schwab, Jessica, Florian Giesert, Benedict Rauser, Chu Lan Lao, Sina Hembach, Sandrine Lefort, Ignacio L Ibarra, et al. 2022. "Parkinson's Disease Motor Symptoms Rescue by CRISPRa-reprogramming Astrocytes into GABAergic Neurons." *EMBO Molecular Medicine*, 1–20. https://doi.org/10.15252/emmm.202114797.
Götz, Magdalena, Swetlana Sirko, Johannes Beckers, and Martin Irmler. 2015. "Reactive Astrocytes as Neural Stem or Progenitor Cells: In Vivo Lineage, In Vitro Potential, and Genome-Wide Expression Analysis." *GLIA*. https://doi.org/10.1002/glia.22850.
Grande, Andrew, Kyoko Sumiyoshi, Alejandro López-Juárez, Jennifer Howard, Bhuvaneswari Sakthivel, Bruce Aronow, Kenneth Campbell, and Masato Nakafuku. 2013. "Environmental Impact on Direct Neuronal Reprogramming in Vivo in the Adult Brain." *Nature Communications* 4. https://doi.org/10.1038/ncomms3373.
Gross, Robert E., Mark F. Mehler, Peter C. Mabie, Ziying Zang, Linda Santschi, and John A. Kessler. 1996. "Bone Morphogenetic Proteins Promote Astroglial Lineage Commitment by Mammalian Subventricular Zone Progenitor Cells." *Neuron*. https://doi.org/10.1016/S0896-6273(00)80193-2.
Guo, Ziyuan, Lei Zhang, Zheng Wu, Yuchen Chen, Fan Wang, and Gong Chen. 2014. "In Vivo Direct Reprogramming of Reactive Glial Cells into Functional Neurons after Brain Injury and in an Alzheimer's Disease Model." *Cell Stem Cell* 14 (2): 188–202.

https://doi.org/10.1016/j.stem.2013.12.001.
Heinrich, Christophe, Robert Blum, Sergio Gascón, Giacomo Masserdotti, Pratibha Tripathi, Rodrigo Sánchez, Steffen Tiedt, Timm Schroeder, Magdalena Götz, and Benedikt Berninger. 2010. "Directing Astroglia from the Cerebral Cortex into Subtype Specific Functional Neurons." *PLoS Biology* 8 (5). https://doi.org/10.1371/journal.pbio.1000373.
Hong, Chen Jei, and Yi Ping Hsueh. 2007. "Cytoplasmic Distribution of T-Box Transcription Factor Tbr-1 in Adult Rodent Brain." *Journal of Chemical Neuroanatomy* 33 (3): 124–30. https://doi.org/10.1016/j.jchemneu.2007.01.005.
Ince-Dunn, Gulayse, Hirotaka J. Okano, Kirk B. Jensen, Woong Yang Park, Ru Zhong, Jernej Ule, Aldo Mele, et al. 2012. "Neuronal Elav-like (Hu) Proteins Regulate RNA Splicing and Abundance to Control Glutamate Levels and Neuronal Excitability." *Neuron*. https://doi.org/10.1016/j.neuron.2012.07.009.
Jiang, Houbo, Zhimin Xu, Ping Zhong, Yong Ren, Gaoyang Liang, Haley A. Schilling, Zihua Hu, et al. 2015. "Cell Cycle and P53 Gate the Direct Conversion of Human Fibroblasts to Dopaminergic Neurons." *Nature Communications*. https://doi.org/10.1038/ncomms10100.
Kang, Wenfei, and Jean M. Hébert. 2011. "Signaling Pathways in Reactive Astrocytes, a Genetic Perspective." *Molecular Neurobiology*. https://doi.org/10.1007/s12035-011-8163-7.
Krueger, Felix. 2015. "Trim Galore!: A Wrapper Tool around Cutadapt and FastQC to Consistently Apply Quality and Adapter Trimming to FastQ Files." *Babraham Institute*.
Kutsche, Lisa K., Deisy M. Gysi, Joerg Fallmann, Kerstin Lenk, Rebecca Petri, Anka Swiersy, Simon D. Klapper, et al. 2018. *No Title*. *Cell Systems*. Vol. 7. Cell Press. https://doi.org/10.1016/j.cels.2018.08.011.
Kwan, Kenneth Y., Nenad Šestan, and E. S. Anton. 2012. "Transcriptional Co-Regulation of Neuronal Migration and Laminar Identity in the Neocortex." *Development*. https://doi.org/10.1242/dev.069963.
Lai, Wi S., Ester Carballo, Judith M. Thorn, Elizabeth A. Kennington, and Perry J. Blackshear. 2000. "Interactions of CCCH Zinc Finger Proteins with MRNA. Binding of Tristetraprolin-Related Zinc Finger Proteins to AU-Rich Elements and Destabilization of MRNA." *Journal of Biological Chemistry*. https://doi.org/10.1074/jbc.M001696200.
Leaman, Sydney, Nicolás Marichal, and Benedikt Berninger. 2022. "Reprogramming Cellular Identity in Vivo." *Development (Cambridge, England)* 149 (4). https://doi.org/10.1242/dev.200433.
Lee, Seong Won, Young Mi Oh, Ya Lin Lu, Woo Kyung Kim, and Andrew S. Yoo. 2018. "MicroRNAs Overcome Cell Fate Barrier by Reducing EZH2-Controlled REST Stability during Neuronal Conversion of Human Adult Fibroblasts." *Developmental Cell* 46 (1): 73-84.e7. https://doi.org/10.1016/j.devcel.2018.06.007.
Li, Xiang, Xiaohan Zuo, Junzhan Jing, Yantao Ma, Jiaming Wang, Defang Liu, Jialiang Zhu, et al. 2015. "Small-Molecule-Driven Direct Reprogramming of Mouse Fibroblasts into Functional Neurons." *Cell Stem Cell* 17 (2): 195–203. https://doi.org/10.1016/j.stem.2015.06.003.
Lu, Ya Lin, Yangjian Liu, Matthew J. McCoy, and Andrew S. Yoo. 2021. "MiR-124 Synergism with ELAVL3 Enhances Target Gene Expression to Promote Neuronal Maturity." *Proceedings of the National Academy of Sciences of the United States of America* 118 (22). https://doi.org/10.1073/pnas.2015454118.
Luján, R., R. Shigemoto, and G. López-Bendito. 2005. "Glutamate and GABA Receptor Signalling in the Developing Brain." *Neuroscience*. https://doi.org/10.1016/j.neuroscience.2004.09.042.
Magnusson, Jens P., Christian Göritz, Jemal Tatarishvili, David O. Dias, Emma M.K. Smith, Olle Lindvall, Zaal Kokaia, and Jonas Frisén. 2014. "A Latent Neurogenic Program in Astrocytes Regulated by Notch Signaling in the Mouse." *Science* 346 (6206): 237–41. https://doi.org/10.1126/science.346.6206.237.
Makeyev, Eugene V., Jiangwen Zhang, Monica A. Carrasco, and Tom Maniatis. 2007. "The MicroRNA MiR-124 Promotes Neuronal Differentiation by Triggering Brain-Specific Alternative Pre-MRNA Splicing." *Molecular Cell* 27 (3): 435–48. https://doi.org/10.1016/j.molcel.2007.07.015.
Martin, Marcel. 2011. "Cutadapt Removes Adapter Sequences from High-Throughput Sequencing Reads." *EMBnet.Journal*. https://doi.org/10.14806/ej.17.1.200.
Matsuda, Taito, Takashi Irie, Shutaro Katsurabayashi, Yoshinori Hayashi, Tatsuya Nagai, Nobuhiko Hamazaki, Aliya Mari D. Adefuin, et al. 2019. "Pioneer Factor NeuroD1 Rearranges Transcriptional and Epigenetic Profiles to Execute Microglia-Neuron Conversion." *Neuron*. https://doi.org/10.1016/j.neuron.2018.12.010.

1058 Mattugini, Nicola, Riccardo Bocchi, Volker Scheuss, Gianluca Luigi Russo, Olof Torper, Chu Lan Lao,
1059 and Magdalena Götz. 2019. "Inducing Different Neuronal Subtypes from Astrocytes in the
1060 Injured Mouse Cerebral Cortex." *Neuron* 103 (6): 1086-1095.e5.
1061 https://doi.org/10.1016/j.neuron.2019.08.009.
1062 Neo, Wen Hao, Karen Yap, Suet Hoay Lee, Liang Sheng Looi, Piyush Khandelia, Sheng Xiong Neo,
1063 Eugene V. Makeyev, and I. Hsin Su. 2014. "MicroRNA MiR-124 Controls the Choice between
1064 Neuronal and Astrocyte Differentiation by Fine-Tuning Ezh2 Expression." *Journal of Biological*
1065 *Chemistry* 289 (30): 20788–801. https://doi.org/10.1074/jbc.M113.525493.
1066 Niu, Wenze, Tong Zang, Yuhua Zou, Sanhua Fang, Derek K. Smith, Robert Bachoo, and Chun Li Zhang.
1067 2013. "In Vivo Reprogramming of Astrocytes to Neuroblasts in the Adult Brain." *Nature Cell*
1068 *Biology*. https://doi.org/10.1038/ncb2843.
1069 Paraskevopoulou, Maria D., Dimitra Karagkouni, Ioannis S. Vlachos, Spyros Tastsoglou, and Artemis G.
1070 Hatzigeorgiou. 2018. "MicroCLIP Super Learning Framework Uncovers Functional
1071 Transcriptome-Wide MiRNA Interactions." *Nature Communications*.
1072 https://doi.org/10.1038/s41467-018-06046-y.
1073 Pataskar, Abhijeet, Johannes Jung, Pawel Smialowski, Florian Noack, Federico Calegari, Tobias Straub,
1074 and Vijay K Tiwari. 2016. "NeuroD1 Reprograms Chromatin and Transcription Factor Landscapes
1075 to Induce the Neuronal Program." *The EMBO Journal*.
1076 https://doi.org/10.15252/embj.201591206.
1077 Petrik, David, Yindi Jiang, Shari G. Birnbaum, Craig M. Powell, Mi-Sung Kim, Jenny Hsieh, and Amelia J.
1078 Eisch. 2012. "Functional and Mechanistic Exploration of an Adult Neurogenesis-promoting Small
1079 Molecule." *The FASEB Journal* 26 (8): 3148–62. https://doi.org/10.1096/fj.11-201426.
1080 Pimentel, Harold, Nicolas L. Bray, Suzette Puente, Páll Melsted, and Lior Pachter. 2017. "Differential
1081 Analysis of RNA-Seq Incorporating Quantification Uncertainty." *Nature Methods*.
1082 https://doi.org/10.1038/nmeth.4324.
1083 Qian, Hao, Xinjiang Kang, Jing Hu, Dongyang Zhang, Zhengyu Liang, Fan Meng, Xuan Zhang, et al.
1084 2020. "Reversing a Model of Parkinson's Disease with in Situ Converted Nigral Neurons."
1085 *Nature*. https://doi.org/10.1038/s41586-020-2388-4.
1086 Rivetti Di Val Cervo, Pia, Roman A. Romanov, Giada Spigolon, Débora Masini, Elisa Martín-Montañez,
1087 Enrique M. Toledo, Gioele La Manno, et al. 2017. "Induction of Functional Dopamine Neurons
1088 from Human Astrocytes in Vitro and Mouse Astrocytes in a Parkinson's Disease Model." *Nature*
1089 *Biotechnology*. https://doi.org/10.1038/nbt.3835.
1090 Sanuki, Rikako, Akishi Onishi, Chieko Koike, Rieko Muramatsu, Satoshi Watanabe, Yuki Muranishi,
1091 Shoichi Irie, et al. 2011. "MiR-124a Is Required for Hippocampal Axogenesis and Retinal Cone
1092 Survival through Lhx2 Suppression." *Nature Neuroscience*. https://doi.org/10.1038/nn.2897.
1093 Scheckel, Claudia, Elodie Drapeau, Maria A. Frias, Christopher Y. Park, John Fak, Ilana Zucker-Scharff,
1094 Yan Kou, et al. 2016. "Regulatory Consequences of Neuronal ELAV-like Protein Binding to Coding
1095 and Non-Coding RNAs in Human Brain." *ELife*. https://doi.org/10.7554/eLife.10421.
1096 Schneider, Jay W., Zhengliang Gao, Shijie Li, Midhat Farooqi, Tie Shan Tang, Ilya Bezprozvanny, Doug
1097 E. Frantz, and Jenny Hsieh. 2008. "Small-Molecule Activation of Neuronal Cell Fate." *Nature*
1098 *Chemical Biology* 4 (7): 408–10. https://doi.org/10.1038/nchembio.95.
1099 Torper, Olof, Ulrich Pfisterer, Daniel A. Wolf, Maria Pereira, Shong Lau, Johan Jakobsson, Anders
1100 Björklund, Shane Grealish, and Malin Parmar. 2013. "Generation of Induced Neurons via Direct
1101 Conversion in Vivo." *Proceedings of the National Academy of Sciences of the United States of*
1102 *America* 110 (17): 7038–43. https://doi.org/10.1073/pnas.1303829110.
1103 Victor, Matheus B., Michelle Richner, Tracey O. Hermanstyne, Joseph L. Ransdell, Courtney Sobieski,
1104 Pan Yue Deng, Vitaly A. Klyachko, Jeanne M. Nerbonne, and Andrew S. Yoo. 2014. "Generation
1105 of Human Striatal Neurons by MicroRNA-Dependent Direct Conversion of Fibroblasts." *Neuron*.
1106 https://doi.org/10.1016/j.neuron.2014.10.016.
1107 Victor, Matheus B., Michelle Richner, Hannah E. Olsen, Seong Won Lee, Alejandro M. Monteys,
1108 Chunyu Ma, Christine J. Huh, et al. 2018. "Striatal Neurons Directly Converted from
1109 Huntington's Disease Patient Fibroblasts Recapitulate Age-Associated Disease Phenotypes."
1110 *Nature Neuroscience*. https://doi.org/10.1038/s41593-018-0075-7.
1111 Visvanathan, Jaya, Seunghee Lee, Bora Lee, Jae W. Lee, and Soo Kyung Lee. 2007. "The MicroRNA
1112 MiR-124 Antagonizes the Anti-Neural REST/SCP1 Pathway during Embryonic CNS
1113 Development." *Genes and Development*. https://doi.org/10.1101/gad.1519107.
1114 Vogel, Katharina U., Lewis S. Bell, Alison Galloway, Helena Ahlfors, and Martin Turner. 2016. "The

RNA-Binding Proteins Zfp36l1 and Zfp36l2 Enforce the Thymic β-Selection Checkpoint by Limiting DNA Damage Response Signaling and Cell Cycle Progression." *The Journal of Immunology*. https://doi.org/10.4049/jimmunol.1600854.

Volvert, Marie Laure, Pierre Paul Prévot, Pierre Close, Sophie Laguesse, Sophie Pirotte, James Hemphill, Florence Rogister, et al. 2014. "MicroRNA Targeting of CoREST Controls Polarization of Migrating Cortical Neurons." *Cell Reports*. https://doi.org/10.1016/j.celrep.2014.03.075.

Wang, Lei Lei, Carolina Serrano, Xiaoling Zhong, Shuaipeng Ma, Yuhua Zou, and Chun Li Zhang. 2021. "Revisiting Astrocyte to Neuron Conversion with Lineage Tracing in Vivo." *Cell*. https://doi.org/10.1016/j.cell.2021.09.005.

Weng, Qinjie, Jincheng Wang, Jiajia Wang, Danyang He, Zuolin Cheng, Feng Zhang, Ravinder Verma, et al. 2019. "Single-Cell Transcriptomics Uncovers Glial Progenitor Diversity and Cell Fate Determinants during Development and Gliomagenesis." *Cell Stem Cell*. https://doi.org/10.1016/j.stem.2019.03.006.

Weyn-Vanhentenryck, Sebastien M., Aldo Mele, Qinghong Yan, Shuying Sun, Natalie Farny, Zuo Zhang, Chenghai Xue, et al. 2014. "HITS-CLIP and Integrative Modeling Define the Rbfox Splicing-Regulatory Network Linked to Brain Development and Autism." *Cell Reports*. https://doi.org/10.1016/j.celrep.2014.02.005.

Wohl, Stefanie Gabriele, and Thomas Andrew Reh. 2016. "MiR-124-9-9* Potentiates Ascl1-Induced Reprogramming of Cultured Müller Glia." *GLIA*. https://doi.org/10.1002/glia.22958.

Wu, Thomas D., and Serban Nacu. 2010. "Fast and SNP-Tolerant Detection of Complex Variants and Splicing in Short Reads." *Bioinformatics*. https://doi.org/10.1093/bioinformatics/btq057.

Wu, Zheng, Matthew Parry, Xiao Yi Hou, Min Hui Liu, Hui Wang, Rachel Cain, Zi Fei Pei, et al. 2020. "Gene Therapy Conversion of Striatal Astrocytes into GABAergic Neurons in Mouse Models of Huntington's Disease." *Nature Communications*. https://doi.org/10.1038/s41467-020-14855-3.

Xue, Yuanchao, Kunfu Ouyang, Jie Huang, Yu Zhou, Hong Ouyang, Hairi Li, Gang Wang, et al. 2013. "Direct Conversion of Fibroblasts to Neurons by Reprogramming PTB-Regulated MicroRNA Circuits." *Cell* 152 (1–2): 82–96. https://doi.org/10.1016/j.cell.2012.11.045.

Yang, Chunzhang, Rajiv R. Iyer, Albert C.H. Yu, Raymund L. Yong, Deric M. Park, Robert J. Weil, Barbara Ikejiri, Roscoe O. Brady, Russell R. Lonser, and Zhengping Zhuang. 2012. "β-Catenin Signaling Initiates the Activation of Astrocytes and Its Dysregulation Contributes to the Pathogenesis of Astrocytomas." *Proceedings of the National Academy of Sciences of the United States of America*. https://doi.org/10.1073/pnas.1118754109.

Yeom, Kyu Hyeon, Simon Mitchell, Anthony J. Linares, Sika Zheng, Chia Ho Lin, Xiao Jun Wang, Alexander Hoffmann, and Douglas L. Black. 2018. "Polypyrimidine Tract-Binding Protein Blocks MiRNA-124 Biogenesis to Enforce Its Neuronal-Specific Expression in the Mouse." *Proceedings of the National Academy of Sciences of the United States of America*. https://doi.org/10.1073/pnas.1809609115.

Yoo, Andrew S., Brett T. Staahl, Lei Chen, and Gerald R. Crabtree. 2009. "MicroRNA-Mediated Switching of Chromatin-Remodelling Complexes in Neural Development." *Nature*. https://doi.org/10.1038/nature08139.

Yoo, Andrew S., Alfred X. Sun, Li Li, Aleksandr Shcheglovitov, Thomas Portmann, Yulong Li, Chris Lee-Messer, Ricardo E. Dolmetsch, Richard W. Tsien, and Gerald R. Crabtree. 2011. "MicroRNA-Mediated Conversion of Human Fibroblasts to Neurons." *Nature*. https://doi.org/10.1038/nature10323.

Yuzwa, Scott A., Michael J. Borrett, Brendan T. Innes, Anastassia Voronova, Troy Ketela, David R. Kaplan, Gary D. Bader, and Freda D. Miller. 2017. "Developmental Emergence of Adult Neural Stem Cells as Revealed by Single-Cell Transcriptional Profiling." *Cell Reports*. https://doi.org/10.1016/j.celrep.2017.12.017.

Zhang, Lei, Jiu Chao Yin, Hana Yeh, Ning Xin Ma, Grace Lee, Xiangyun Amy Chen, Yanming Wang, et al. 2015. "Small Molecules Efficiently Reprogram Human Astroglial Cells into Functional Neurons." *Cell Stem Cell* 17 (6): 735–47. https://doi.org/10.1016/j.stem.2015.09.012.

Zhang, Ye, Kenian Chen, Steven A. Sloan, Mariko L. Bennett, Anja R. Scholze, Sean O'Keeffe, Hemali P. Phatnani, et al. 2014. "An RNA-Sequencing Transcriptome and Splicing Database of Glia, Neurons, and Vascular Cells of the Cerebral Cortex." *Journal of Neuroscience*. https://doi.org/10.1523/JNEUROSCI.1860-14.2014.

Zhou, Haibo, Jinlin Su, Xinde Hu, Changyang Zhou, He Li, Zhaorong Chen, Qingquan Xiao, et al. 2020. "Glia-to-Neuron Conversion by CRISPR-CasRx Alleviates Symptoms of Neurological Disease in

1172 Mice." *Cell*. https://doi.org/10.1016/j.cell.2020.03.024.
1173

1174

Figure 1

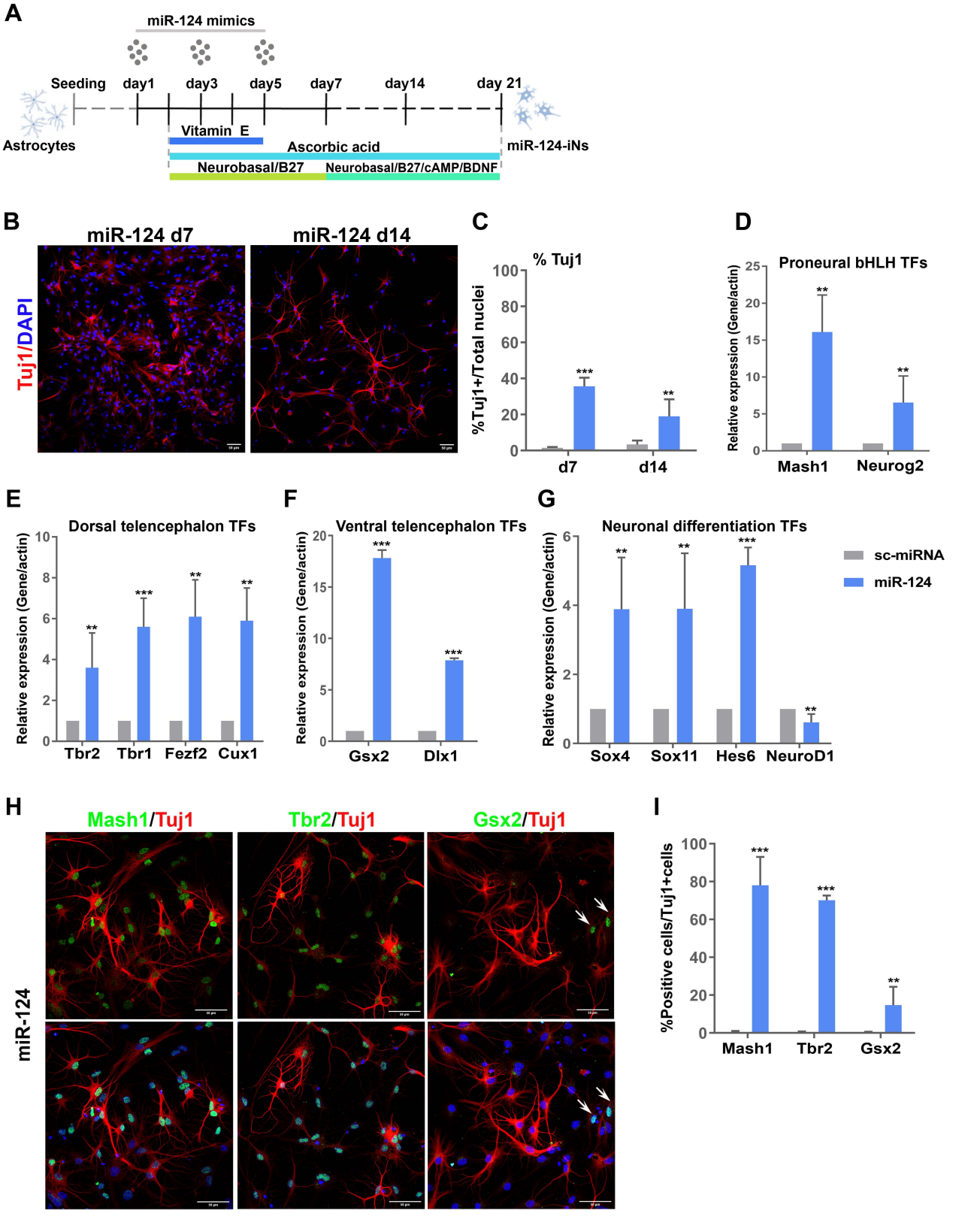
A
miR-124 mimics
Seeding
day1
day3
day5
day7
day14
day 21
Astrocytes
Vitamin E
Ascorbic acid
miR-124-iNs
Neurobasal/B27
Neurobasal/B27/cAMP/BDNF
B
miR-124 d7
miR-124 d14
Tuj1/DAPI
C
% Tuj1
%Tuj1+/Total nuclei
d7
d14
D
Proneural bHLH TFs
Relative expression (Gene/actin)
Mash1
Neurog2
E
Dorsal telencephalon TFs
Relative expression (Gene/actin)
Tbr2
Tbr1
Fezf2
Cux1
F
Ventral telencephalon TFs
Relative expression (Gene/actin)
Gsx2
Dlx1
G
Neuronal differentiation TFs
Relative expression (Gene/actin)
Sox4
Sox11
Hes6
NeuroD1
sc-miRNA
miR-124
H
Mash1/Tuj1
Tbr2/Tuj1
Gsx2/Tuj1
miR-124
I
%Positive cells/Tuj1+cells
Mash1
Tbr2
Gsx2

1175 # Figures

1176 **Figure 1: miR-124 is sufficient to instruct reprogramming of postnatal cortical astrocytes to**
1177 **iNs**

1178 **(A)** Overview of the miR-124-mediated reprogramming protocol. **(B)** Immunostaining of
1179 astrocytes reprogrammed with miR-124 at d7 and d14 of the reprogramming protocol with
1180 anti-Tuj1 antibody. **(C)** Quantification of the percentage of Tuj1+ reprogrammed cells (average
1181 ±SD, n=4 independent experiments). RT-qPCR analysis of the mRNA levels of the proneural
1182 TFs, *Mash1* and *Neurog2* **(D)**, the dorsal telencephalon TFs, *Tbr2, Tbr1, Fezf2, Cux1* **(E)**, the
1183 ventral telencephalon *TFs, Gsx2* and *Dlx1* **(F),** and the neuronal differentiation TFs, *Sox4,*
1184 *Sox11, Hes6* and *NeuroD1* **(G)**. Data are presented as fold change *vs* sc-miRNA (average ± SD,
1185 n=3 independent experiments). **(H)** Co-immunostaining of astrocytes reprogrammed with
1186 miR-124 at d7 of the reprogramming protocol with anti-Mash1/Tuj1, anti-Tbr2/Tuj1 and anti-
1187 Gsx2/Tuj1 antibodies. **(I)** Quantification of the percentage of Mash1+, Tbr2+ and Gsx2+ in
1188 Tuj1+ reprogrammed cells (average ± SD, n=3 independent experiments). For all presented
1189 data **p<0.01 and ***p<0.001 vs sc-miRNA.

1190

Figure 2

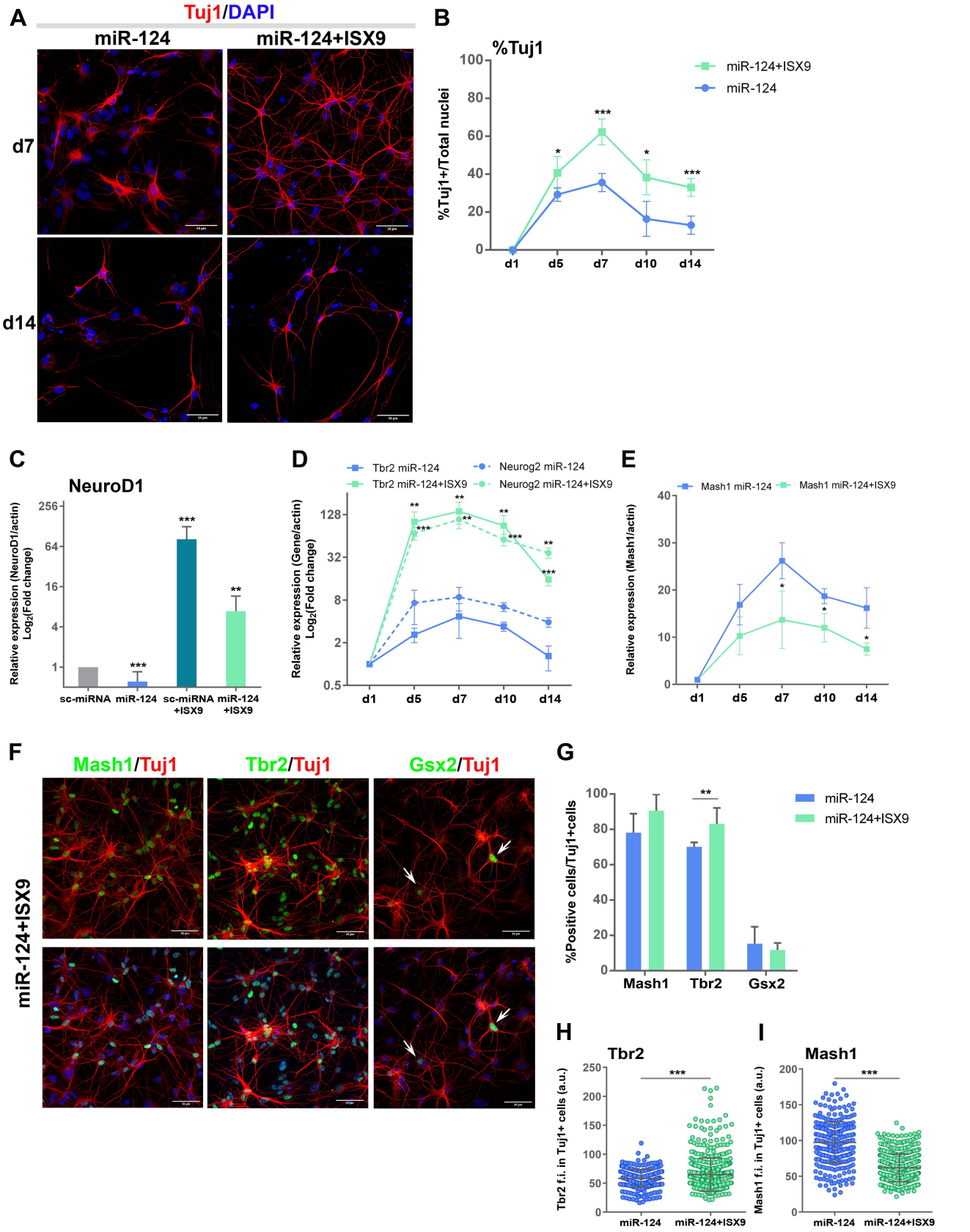
A
Tuj1/DAPI
miR-124
miR-124+ISX9
d7
d14
B
%Tuj1
%Tuj1+/Total nuclei
miR-124+ISX9
miR-124
d1
d5
d7
d10
d14
C
NeuroD1
Relative expression (NeuroD1/actin)
Log2(Fold change)
sc-miRNA
miR-124
sc-miRNA +ISX9
miR-124 +ISX9
D
Tbr2 miR-124
Tbr2 miR-124+ISX9
Neurog2 miR-124
Neurog2 miR-124+ISX9
Relative expression (Gene/actin)
Log2(Fold change)
E
Mash1 miR-124
Mash1 miR-124+ISX9
Relative expression (Mash1/actin)
F
Mash1/Tuj1
Tbr2/Tuj1
Gsx2/Tuj1
miR-124+ISX9
G
%Positive cells/Tuj1+cells
miR-124
miR-124+ISX9
Mash1
Tbr2
Gsx2
H
Tbr2
Tbr2 f.i. in Tuj1+ cells (a.u.)
miR-124
miR-124+ISX9
I
Mash1
Mash1 f.i. in Tuj1+ cells (a.u.)
miR-124
miR-124+ISX9

1191 **Figure 2: The neurogenic compound ISX9 greatly enhances the miR-124-induced**
1192 **reprogramming efficiency and differentiation state of iNs**

1193 **(A)** Immunostaining of astrocytes reprogrammed with miR-124 or miR-124+ISX9 at d7 and d14
1194 of the reprogramming protocol with anti-Tuj1 antibody. **(B)** Quantification of the percentage
1195 of Tuj1+ reprogrammed cells at the time points d1, d5, d7, d10 and d14 of the reprogramming
1196 protocol (average ± SD, n=3 independent experiments for d5 and d10, n=8 for d7 and n=4 for
1197 d14, *p<0.05 and ***p<0.001 *vs* miR-124). **(C)** RT-qPCR analysis of the mRNA levels of
1198 NeuroD1 at d7 of the reprogramming protocol. Data are presented as $\log_2$ (fold change) *vs* sc-
1199 miRNA (average ± SD, n=3 independent experiments, **p<0.01 and ***p<0.001 *vs* sc-miRNA).
1200 RT-qPCR analysis of the mRNA levels of the TFs, Neurog2 and Tbr2 **(D)** and Mash1 **(E)** at the
1201 time points d1, d5, d7, d10 and d14 of the reprogramming protocol. Data are presented as
1202 $\log_2$(fold change) (**D**) and fold change (**E**) *vs* astrocytes (d1) (average ± SD, n=3 independent
1203 experiments, *p<0.05, **p<0.01 and ***p<0.001 *vs* miR-124). **(F)** Co-immunostaining of
1204 astrocytes reprogrammed with miR-124+ISX9 at d7 of the reprogramming protocol with anti-
1205 Mash1/Tuj1, anti-Tbr2/Tuj1 and anti-Gsx2/Tuj1 antibodies. **(G)** Quantification of the
1206 percentage of Mash1+, Tbr2+ and Gsx2+ in Tuj1+ reprogrammed cells either with miR-124 or
1207 miR-124+ISX9 at d7 (average ± SD, n=3 independent experiments, **p<0.01 *vs* miR-124).
1208 Measurement of the mean nuclear fluorescence intensity of Tbr2 **(H)** and Mash1 **(I)** in Tuj1+
1209 reprogrammed cells either with miR-124 or miR-124+ISX9 at d7 (co-immunostaining with anti-
1210 Tbr2/Mash1/Tuj1 antibodies). A representative experiment is shown of n=3 independent
1211 experiments (mean ± SD, n=326 cells for miR-124 and n=540 cells for miR-124+ISX9,
1212 ***p<0.001 *vs* miR-124).

1213

Figure 3

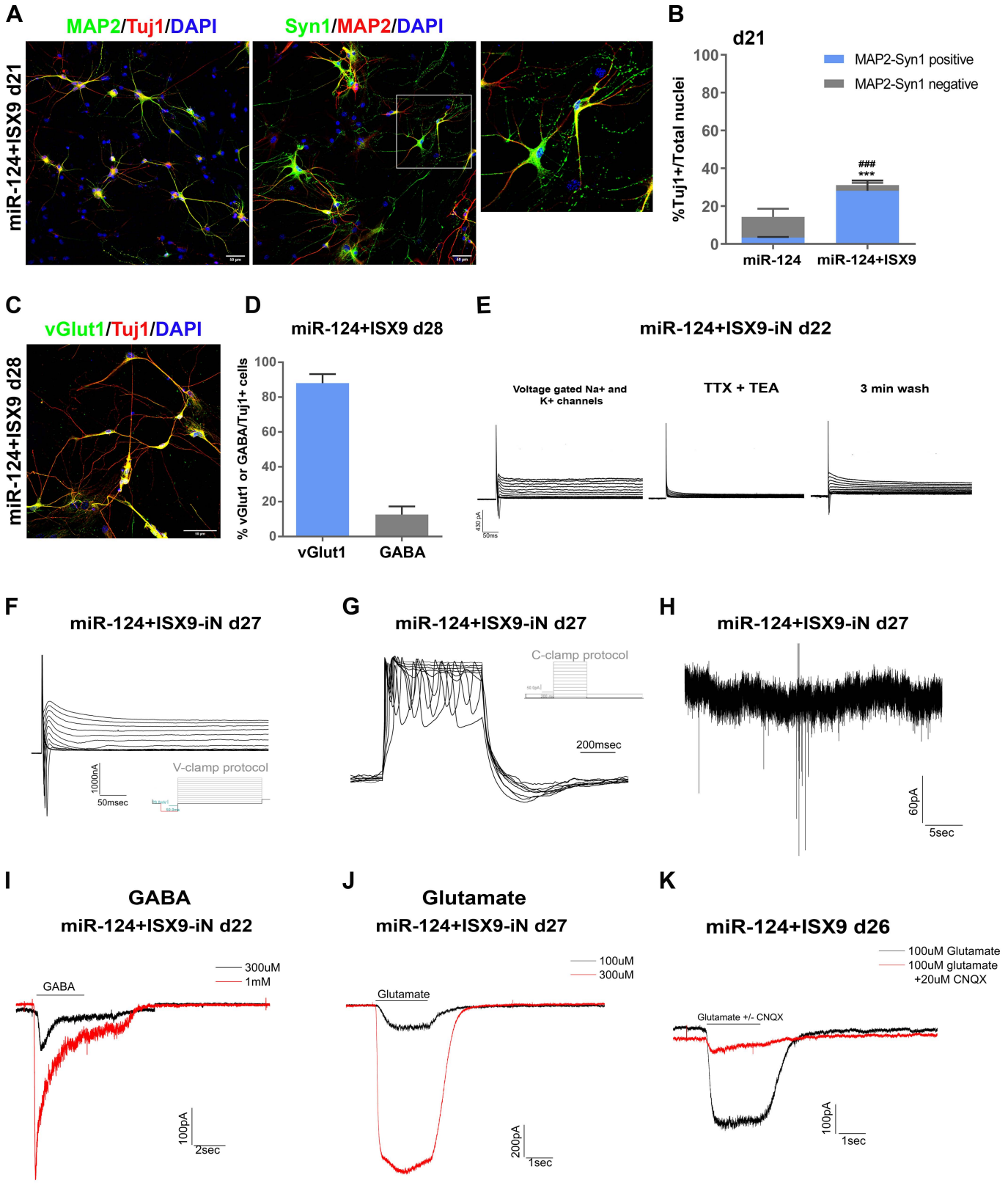
A
MAP2/Tuj1/DAPI
Syn1/MAP2/DAPI
miR-124+ISX9 d21
B
d21
MAP2-Syn1 positive
MAP2-Syn1 negative
%Tuj1+/Total nuclei
100
80
60
40
20
0
###
***
miR-124
miR-124+ISX9
C
vGlut1/Tuj1/DAPI
miR-124+ISX9 d28
D
miR-124+ISX9 d28
% vGlut1 or GABA/Tuj1+ cells
100
80
60
40
20
0
vGlut1
GABA
E
miR-124+ISX9-iN d22
Voltage gated Na+ and K+ channels
TTX + TEA
3 min wash
50ms
F
miR-124+ISX9-iN d27
1000nA
50msec
V-clamp protocol
G
miR-124+ISX9-iN d27
C-clamp protocol
200msec
H
miR-124+ISX9-iN d27
60pA
5sec
I
GABA
miR-124+ISX9-iN d22
300uM
1mM
GABA
100pA
2sec
J
Glutamate
miR-124+ISX9-iN d27
100uM
300uM
Glutamate
200pA
1sec
K
miR-124+ISX9 d26
100uM Glutamate
100uM glutamate +20uM CNQX
Glutamate +/- CNQX
100pA
1sec

1214 **Figure 3: miR-124+ISX9-iNs exhibit characteristics of mature, electrophysiologically active**
1215 **neurons**

1216 **(A)** Co-immunostaining of miR-124+ISX9-iNs at d21 of the reprogramming protocol with anti-
1217 MAP2/Tuj1 and anti-MAP2/Synapsin1 antibodies. Inset area indicated in white frame. **(B)**
1218 Quantification of the percentage of Tuj1+ miR-124-iNs and miR-124+ISX9-iNs at d21 of the
1219 reprogramming protocol. The percentage of MAP2/Syn1 double positive (DP) Tuj1+ iNs is
1220 shown in blue (average ± SD, n=3 independent experiments, ***$p<0.001$ refers to
1221 %MAP2/Syn1 DP in Tuj1+ miR-124+ISX9-iNs *vs* miR-124-iNs and $^{###}p<0.001$ refers to %Tuj1
1222 miR-124+ISX9-iNs *vs* miR-124-iNs). **(C)** Co-immunostaining of miR-124+ISX9-iNs at d28 of the
1223 reprogramming protocol with anti-vGlut1/Tuj1 antibodies. **(D)** Quantification of the
1224 percentage of vGlut1+/Tuj1+ and GABA+/Tuj1+ miR-124+ISX9-iNs at d28 (average ± SD, n=3
1225 independent experiments). **(E)** Superimposed traces of inward Na^+ currents and outward K^+
1226 currents evoked by depolarizing voltage steps obtained from a miR-124+ISX9-iN (d22) (left
1227 panel). Superimposed traces of inward and outward currents evoked by the same protocol
1228 after 1 min pre-application of 1µM TTX + 10mM TEA, showing the inhibition of both inward
1229 and outward currents (middle panel), followed by full recovery of the current traces after 3
1230 min wash of the cell (right panel). **(F)** Superimposed traces of inward Na^+ currents and
1231 outward K^+ currents evoked by depolarizing voltage steps obtained from a miR-124+ISX9-iN
1232 (d27). **(G)** Example of a repetitive action potential induced from a mature miR-124+ISX9-iN
1233 (d27) by different current steps (injections) at the current clamp mode (the protocol of
1234 current clamp is shown upper right). (**H**) Example of a mature miR-124+ISX9-iN (d27) that
1235 exhibits spontaneous post-synaptic activity at -70 mV holding potential. Representative
1236 traces of ionic currents induced by application of the neurotransmitter GABA in two different
1237 concentrations (300µM and 1mM) obtained from a miR-124+ISX9-iN in the early stage of
1238 neuronal maturation (d22) **(I)** and the neurotransmitter glutamate in two different
1239 concentrations (100µM and 300µM) obtained from a miR-124+ISX9-iN in the late stage of
1240 maturation (d27) **(J)**.The cell membrane potential was held at -70 mV and the time of agonist
1241 application is indicated in bars above the traces. **(K)** Superimposed traces obtained from a
1242 mature miR-124+ISX9-iN (d26) with application of 100 µM glutamate (Glut) or co-application
1243 of 100µM Glut+CNQX indicated that the antagonist CNQX inhibits the AMPA/ kainite
1244 glutamate receptor.

1245

Figure 4

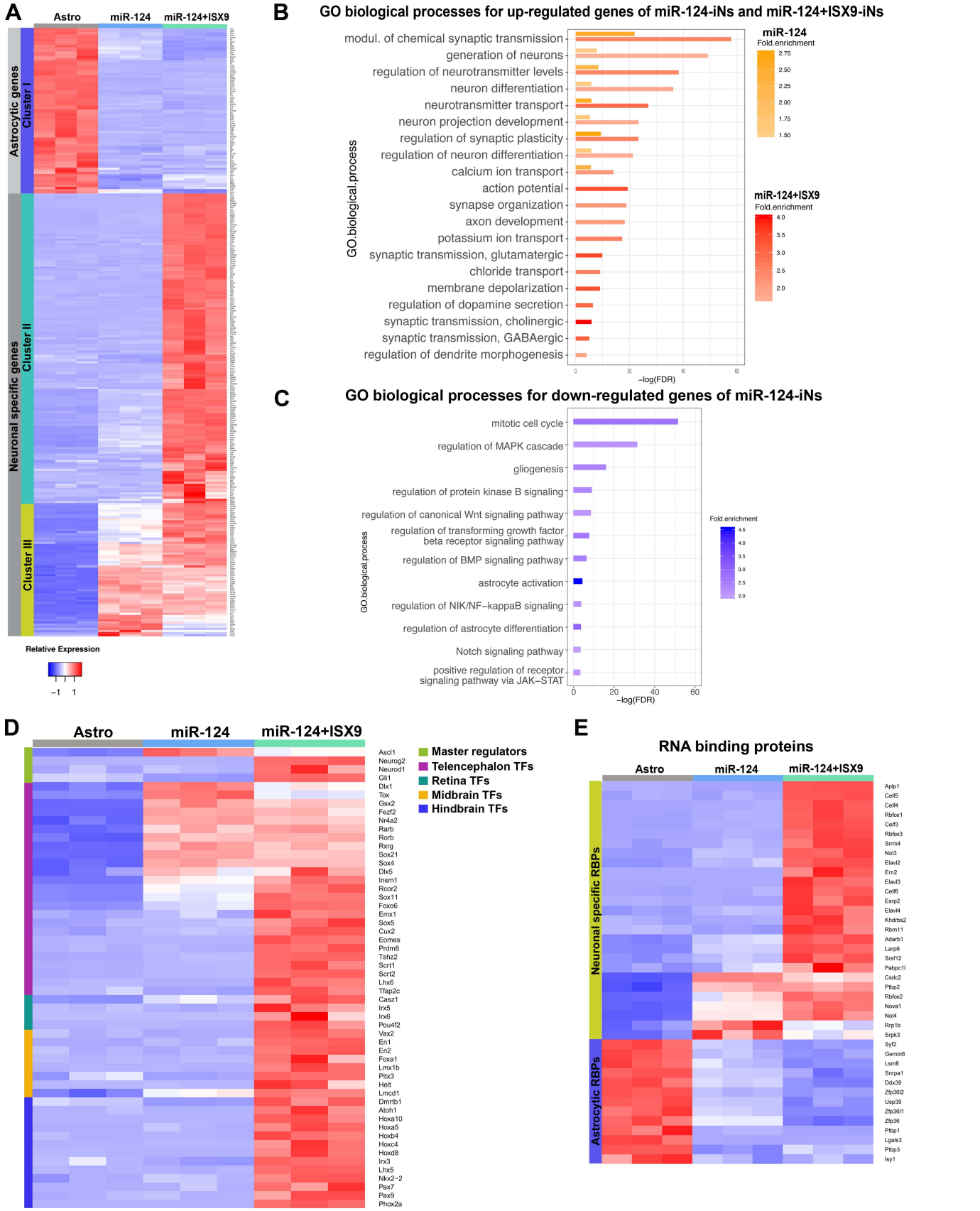
A
Astro
miR-124
miR-124+ISX9
Astrocytic genes
Cluster I
Neuronal specific genes
Cluster II
Cluster III
Relative Expression
−1
1
B
GO biological processes for up-regulated genes of miR-124-iNs and miR-124+ISX9-iNs
modul. of chemical synaptic transmission
generation of neurons
regulation of neurotransmitter levels
neuron differentiation
neurotransmitter transport
neuron projection development
regulation of synaptic plasticity
regulation of neuron differentiation
calcium ion transport
action potential
synapse organization
axon development
potassium ion transport
synaptic transmission, glutamatergic
chloride transport
membrane depolarization
regulation of dopamine secretion
synaptic transmission, cholinergic
synaptic transmission, GABAergic
regulation of dendrite morphogenesis
GO.biological.process
−log(FDR)
miR-124
Fold.enrichment
2.75
2.50
2.25
2.00
1.75
1.50
miR-124+ISX9
Fold.enrichment
4.0
3.5
3.0
2.5
2.0
C
GO biological processes for down-regulated genes of miR-124-iNs
mitotic cell cycle
regulation of MAPK cascade
gliogenesis
regulation of protein kinase B signaling
regulation of canonical Wnt signaling pathway
regulation of transforming growth factor beta receptor signaling pathway
regulation of BMP signaling pathway
astrocyte activation
regulation of NIK/NF−kappaB signaling
regulation of astrocyte differentiation
Notch signaling pathway
positive regulation of receptor signaling pathway via JAK−STAT
GO.biological.process
−log(FDR)
Fold.enrichment
4.5
4.0
3.5
3.0
2.5
2.0
D
Astro
miR-124
miR-124+ISX9
Ascl1
Neurog2
Neurod1
Gli1
Dlx1
Tox
Gsx2
Fezf2
Nr4a2
Rarb
Rorb
Rxrg
Sox21
Sox4
Dlx5
Insm1
Rcor2
Sox11
Foxo6
Emx1
Sox5
Cux2
Eomes
Prdm8
Tshz2
Scrt1
Scrt2
Lhx6
Tfap2c
Casz1
Irx5
Irx6
Pou4f2
Vax2
En1
En2
Foxa1
Lmx1b
Pitx3
Helt
Lmcd1
Dmrtb1
Atoh1
Hoxa10
Hoxa5
Hoxb4
Hoxc4
Hoxd8
Irx3
Lhx5
Nkx2−2
Pax7
Pax9
Phox2a
Master regulators
Telencephalon TFs
Retina TFs
Midbrain TFs
Hindbrain TFs
E
RNA binding proteins
Astro
miR-124
miR-124+ISX9
Neuronal specific RBPs
Astrocytic RBPs
Aplp1
Celf5
Celf4
Rbfox1
Celf3
Rbfox3
Srrm4
Nol3
Elavl2
Ern2
Elavl3
Celf6
Esrp2
Elavl4
Khdrbs2
Rbm11
Adarb1
Larp6
Srsf12
Pabpc1l
Cadc2
Ptbp2
Rbfox2
Nova1
Nol4
Rrp1b
Srpk3
Syf2
Gemin6
Lsm8
Snrpa1
Ddx39
Zfp36l2
Usp39
Zfp36l1
Zfp36
Ptbp1
Lgals3
Ptbp3
Isy1

1246 **Figure 4: RNA-Seq analysis revealed both independent and cooperative transcriptional**
1247 **contributions of miR-124 and ISX9 in the reprogramming process**

1248 **(A)** Heat map analysis of 300 up- and down-regulated DEGs that belong to the GO terms: Glial
1249 cell differentiation, Gliogenesis, Astrocyte development, Generation of neurons, Neuron
1250 differentiation, Regulation of neuron differentiation, Neurotransmitter transport and Synaptic
1251 signaling. **(B)** GO analysis of biological processes for the up-regulated DEGs in miR-124-iNs *vs*
1252 astro (in orange) and miR-124+ISX9-iNs *vs* astro (in red). **(C)** GO analysis of biological processes
1253 for the down-regulated DEGs in miR-124-iNs *vs* astro. GO terms are ranked according to
1254 $\log_{10}$FDR and the intensity legends indicate the fold enrichment of each GO term. **(D)** Heat
1255 map analysis of 54 up-regulated differentially expressed TFs clustered according to the brain
1256 region they are developmentally expressed (telencephalon, retina, midbrain and hindbrain).
1257 **(E)** Heat map analysis of 40 up- and down-regulated RBPs.

1258

Figure 5

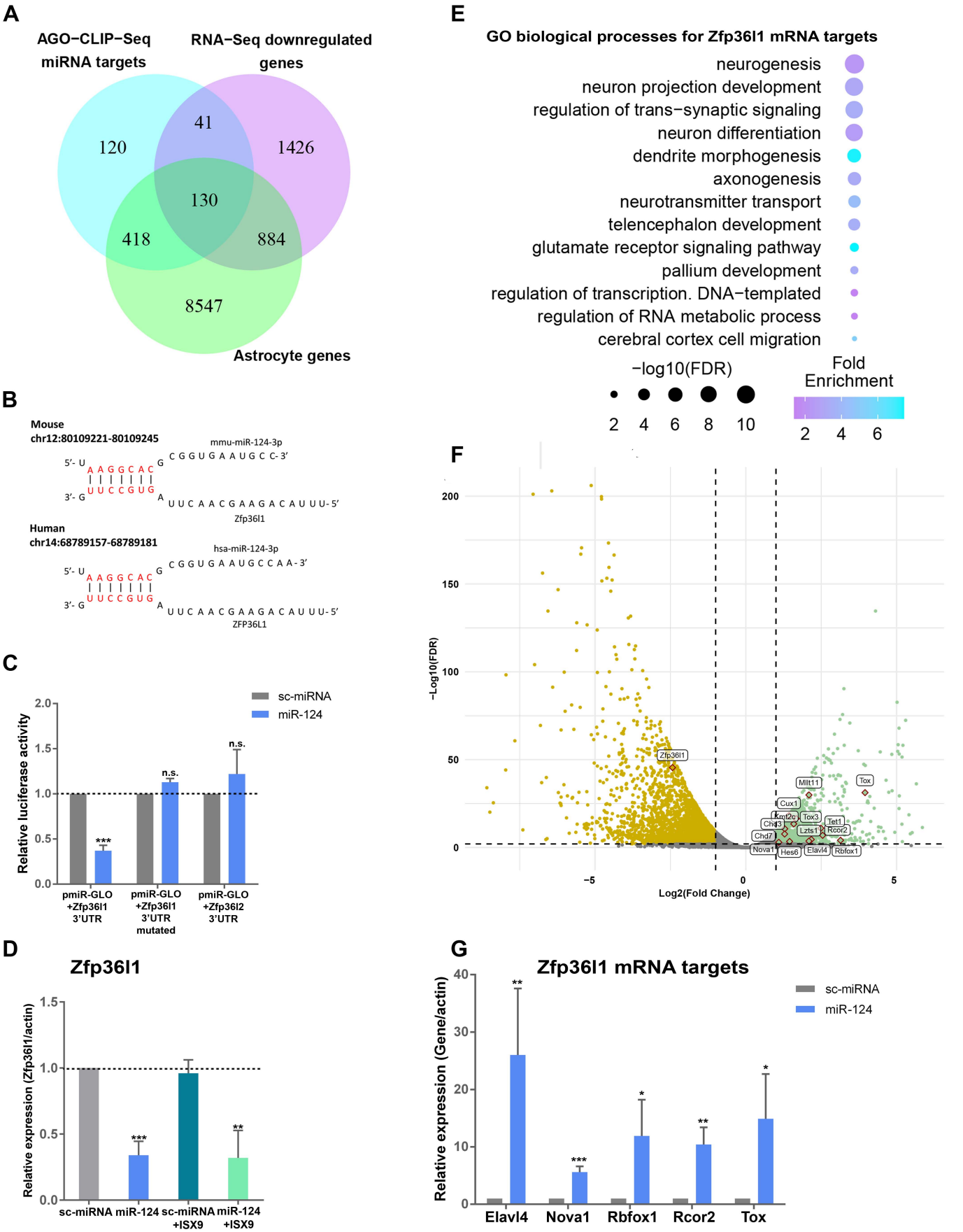
A
AGO−CLIP−Seq miRNA targets
RNA−Seq downregulated genes
Astrocyte genes
120
41
1426
130
418
884
8547
B
Mouse
chr12:80109221-80109245
mmu-miR-124-3p
5′- U
G
C G G U G A A U G C C- 3′
A A G G C A C
U U C C G U G
3′- G
A
U U C A A C G A A G A C A U U U- 5′
Zfp36l1
Human
chr14:68789157-68789181
hsa-miR-124-3p
5′- U
G
C G G U G A A U G C C A A- 3′
A A G G C A C
U U C C G U G
3′- G
A
U U C A A C G A A G A C A U U U- 5′
ZFP36L1
C
sc-miRNA
miR-124
Relative luciferase activity
2.0
1.5
1.0
0.5
0.0
***
n.s.
n.s.
pmiR-GLO +Zfp36l1 3'UTR
pmiR-GLO +Zfp36l1 3'UTR mutated
pmiR-GLO +Zfp36l2 3'UTR
D
Zfp36l1
Relative expression (Zfp36l1/actin)
1.5
1.0
0.5
0.0
***
**
sc-miRNA
miR-124
sc-miRNA +ISX9
miR-124 +ISX9
E
GO biological processes for Zfp36l1 mRNA targets
neurogenesis
neuron projection development
regulation of trans−synaptic signaling
neuron differentiation
dendrite morphogenesis
axonogenesis
neurotransmitter transport
telencephalon development
glutamate receptor signaling pathway
pallium development
regulation of transcription. DNA−templated
regulation of RNA metabolic process
cerebral cortex cell migration
−log10(FDR)
2
4
6
8
10
Fold Enrichment
2
4
6
F
−Log10(FDR)
200
150
100
50
0
Zfp36l1
Mllt11
Tox
Cux1
Kmt2c
Tox3
Chd3
Tet1
Lzts1
Rcor2
Chd7
Nova1
Hes6
Elavl4
Rbfox1
−5
0
5
Log2(Fold Change)
G
Zfp36l1 mRNA targets
Relative expression (Gene/actin)
40
30
20
10
0
sc-miRNA
miR-124
**
***
*
**
*
Elavl4
Nova1
Rbfox1
Rcor2
Tox

1259 **Figure 5: The RNA-binding protein Zfp36l1 is a novel direct target of miR-124**

1260 **(A)** Venn diagram of the miR-124 targets, derived from AGO-HITS-CLIP and the down-
1261 regulated DEGs of miR-124 *vs* sc-miRNA astro RNA-Seq data (log2(fold change)≤-1, FDR<0.01).
1262 Identified miR-124 targets were combined with a public reference list of genes, expressed in
1263 astrocytes, resulting in a set of 130 genes. **(B)** miR-124 direct binding to the 3' UTR of Zfp36l1
1264 and ZFP36L1, in mouse and human species respectively. miR-124 binds with perfect seed
1265 complementarity (7mer-m8 site) in both species. **(C)** Analysis of luciferase activity in HEK293T
1266 cells upon co-transfection with sc-miRNA or miR-124 mimics along with the reporter construct
1267 pmiR-GLO containing the 3'UTR of Zfp36l1 with the miR-124 binding site (n=7 independent
1268 experiments) or the 3'UTR of Zfp36l1 with the mutated miR-124 binding site (n=3) or the
1269 3'UTR of Zfp36l2 (n=6). Normalized Firefly luciferase activity for sc-miRNA has been set to 1,
1270 (average ± SD). **(D)** RT-qPCR validation of the mRNA levels of miR-124 direct target *Zfp36l1* at
1271 d7 (average ±SD, n=3 independent experiments). **(E)** GO analysis of biological processes for
1272 Zfp36l1 direct targets that are also significantly up-regulated in miR-124-iNs *vs* sc-miRNA
1273 astro. GO terms are ranked according to $\log_{10}$FDR and the intensity legend shows the fold
1274 enrichment of each GO term. **(F)** Volcano plot comparing the $\log_2$(fold change) of TPM values
1275 in the miR-124-iNs vs sc-miRNA astro condition versus the $\log_{10}$(FDR) values. Significantly up-
1276 regulated ($\log_2$(fold change)≥1, FDR<0.05) and down-regulated ($\log_2$(fold change)≤-1,
1277 FDR<0.05) genes are shown in green and orange respectively. Labels of Zfp36l1 and neuronal-
1278 specific up-regulated genes that are also Zfp36l1 direct targets are portrayed. **(G)** RT-qPCR
1279 validation of the mRNA levels of the Zfp36l1 targets *Elavl4, Nova1, Rbofox1, Rcor2* and *Tox* at
1280 d7 (average ±SD, n=3 independent experiments). For all data presented *p<0.05, **p<0.01
1281 and ***p<0.001 *vs* sc-miRNA.

1282

Figure 6

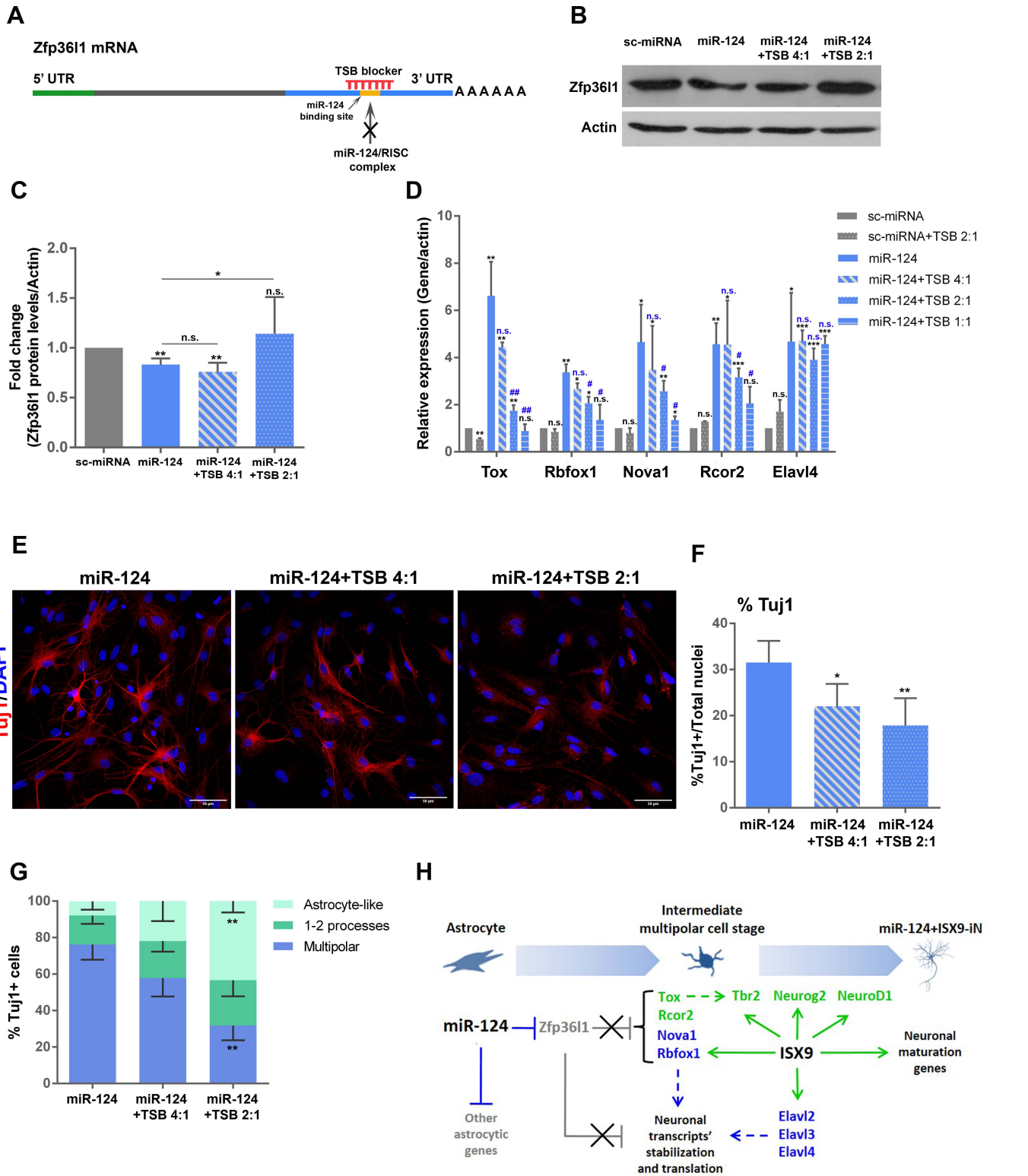
A
Zfp36l1 mRNA
5' UTR
TSB blocker
3' UTR
A A A A A A
miR-124 binding site
miR-124/RISC complex
B
sc-miRNA
miR-124
miR-124 +TSB 4:1
miR-124 +TSB 2:1
Zfp36l1
Actin
C
Fold change (Zfp36l1 protein levels/Actin)
sc-miRNA
miR-124
miR-124 +TSB 4:1
miR-124 +TSB 2:1
D
Relative expression (Gene/actin)
sc-miRNA
sc-miRNA+TSB 2:1
miR-124
miR-124+TSB 4:1
miR-124+TSB 2:1
miR-124+TSB 1:1
Tox
Rbfox1
Nova1
Rcor2
Elavl4
E
miR-124
miR-124+TSB 4:1
miR-124+TSB 2:1
Tuj1/DAPI
F
% Tuj1
%Tuj1+/Total nuclei
miR-124
miR-124 +TSB 4:1
miR-124 +TSB 2:1
G
% Tuj1+ cells
Astrocyte-like
1-2 processes
Multipolar
miR-124
miR-124 +TSB 4:1
miR-124 +TSB 2:1
H
Astrocyte
Intermediate multipolar cell stage
miR-124+ISX9-iN
miR-124
Zfp36l1
Tox
Rcor2
Nova1
Rbfox1
Tbr2
Neurog2
NeuroD1
ISX9
Neuronal maturation genes
Other astrocytic genes
Neuronal transcripts' stabilization and translation
Elavl2
Elavl3
Elavl4

1283 **Figure 6: Targeting of Zfp36l1 by miR-124 plays a key role in the miR-124-induced cell fate**
1284 **switch of astrocytes to iNs**

1285 **(A)** Schematic representation of the TSB binding region in the 3'UTR of *Zfp36l1* mRNA. **(B)**
1286 Western blot analysis of the protein levels of Zfp36l1 in the absence or presence of increasing
1287 concentrations of TSB (miR-124:TSB molecular ratio 4:1 and 2:1) at d5 of the reprogramming
1288 protocol. Actin protein levels have been used as loading control. **(C)** Quantification of Zfp36l1
1289 protein levels normalized to β-actin. Normalized Zfp36l1 protein levels in sc-miRNA
1290 transfected astrocytes have been set to 1, (average ± SD, n=3 independent experiments,
1291 *p<0.05, **p<0.01 *vs* sc-miRNA). **(D)** RT-qPCR analysis of the mRNA levels of the Zfp36l1
1292 targets *Tox, Rbfox1, Nova1, Rcor2* and *Elavl4* in the presence or absence of increasing
1293 concentrations of TSB (miR-124:TSB molecular ratio 4:1, 2:1 and 1:1) at d3 of the
1294 reprogramming protocol (average ± SD, n=3 independent experiments,*p<0.05, **p<0.01
1295 and ***p<0.001 *vs* sc-miRNA and $^{\#}$p<0.05, $^{\#\#}$p<0.01 *vs* miR-124). **(E)** Immunostaining of
1296 astrocytes reprogrammed with miR-124 or miR-124 along with increasing concentrations of
1297 TSB (4:1 and 2:1) with anti-Tuj1 antibody at d5 of the reprogramming protocol. **(F)**
1298 Quantification of the percentage of Tuj1+ cells at d5 (average ±SD, n=3 independent
1299 experiments, *p<0.05 and **p<0.01 *vs* miR-124). **(G)** Morphological characterization of Tuj1+
1300 cells at d5. Quantification of the percentages of multipolar Tuj1+ cells (3 or more processes
1301 extending from soma), Tuj1+ cells with 1-2 processes and Tuj1+ cells with an astrocyte-like
1302 morphology (rectangular soma with none or 1-2 processes) (average ± SD, n=3 independent
1303 experiments, **p<0.01 *vs* miR-124). **(H)** Proposed model of independent and cooperative
1304 transcriptional and post-transcriptional contributions of miR-124 and ISX9 in miR-124/ISX9–
1305 induced direct neuronal conversion of cortical astrocytes. Post-transcriptional events and the
1306 RBPs are highlighted in blue, transcriptional events along with the TFs are shown in green,
1307 while down-regulated genes and (blocked) inhibitory mechanisms are shown in grey, (dashed
1308 lines present knowledge from the literature).

1309

Figure 7

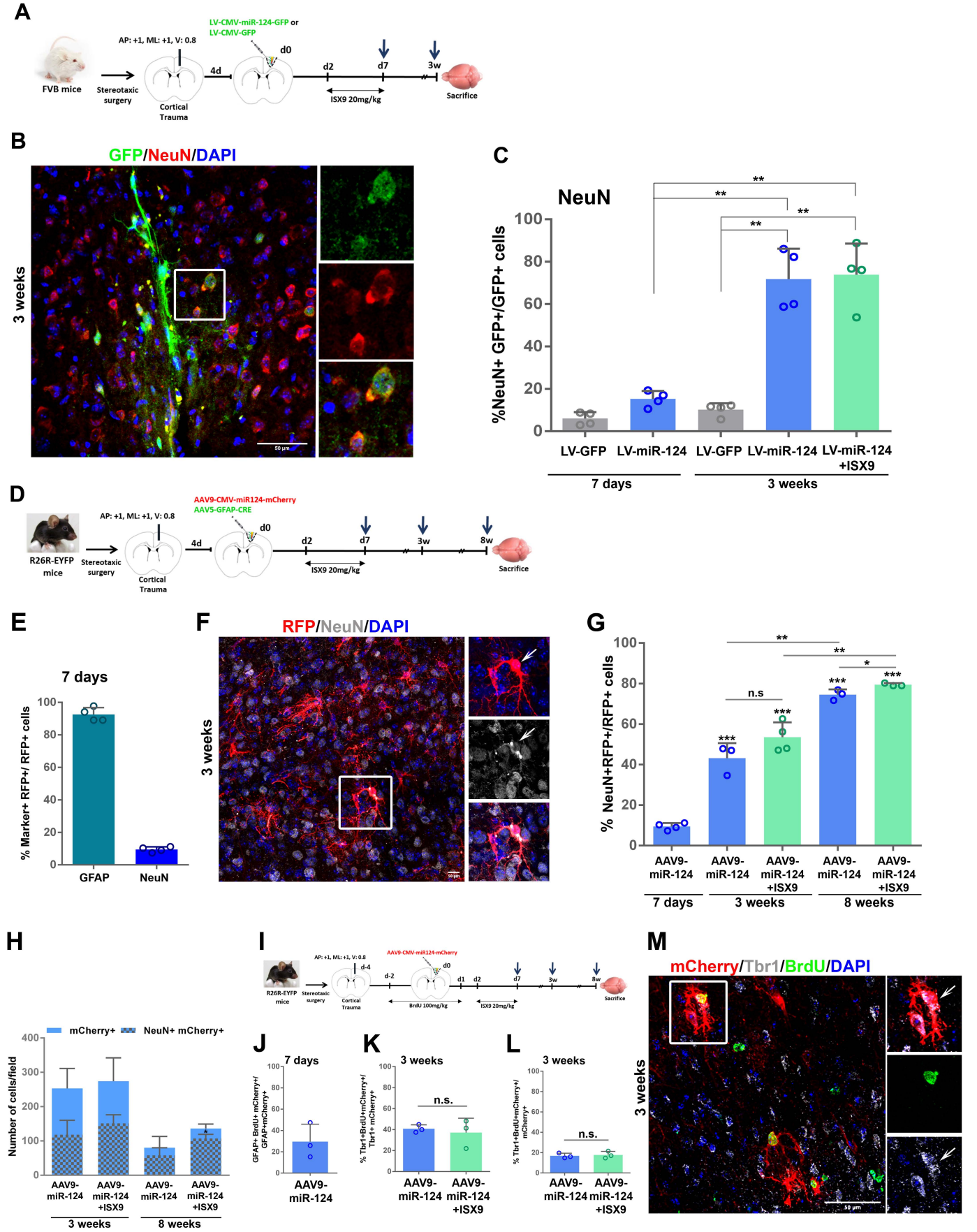
A
FVB mice
Stereotaxic surgery
AP: +1, ML: +1, V: 0.8
Cortical Trauma
4d
LV-CMV-miR-124-GFP or LV-CMV-GFP
d0
d2
d7
3w
ISX9 20mg/kg
Sacrifice
B
GFP/NeuN/DAPI
3 weeks
C
NeuN
%NeuN+ GFP+/GFP+ cells
LV-GFP
LV-miR-124
LV-GFP
LV-miR-124
LV-miR-124 +ISX9
7 days
3 weeks
D
R26R-EYFP mice
Stereotaxic surgery
AP: +1, ML: +1, V: 0.8
Cortical Trauma
4d
AAV9-CMV-miR124-mCherry
AAV5-GFAP-CRE
d0
d2
d7
3w
8w
ISX9 20mg/kg
Sacrifice
E
7 days
% Marker+ RFP+/ RFP+ cells
GFAP
NeuN
F
RFP/NeuN/DAPI
3 weeks
G
% NeuN+RFP+/RFP+ cells
n.s
AAV9-miR-124
AAV9-miR-124 +ISX9
7 days
3 weeks
8 weeks
H
mCherry+
NeuN+ mCherry+
Number of cells/field
AAV9-miR-124
AAV9-miR-124 +ISX9
3 weeks
8 weeks
I
R26R-EYFP mice
Stereotaxic surgery
AP: +1, ML: +1, V: 0.8
Cortical Trauma
AAV9-CMV-miR124-mCherry
d-4
d-2
d0
d1
d2
d7
3w
8w
BrdU 100mg/kg
ISX9 20mg/kg
Sacrifice
J
7 days
GFAP+ BrdU+ mCherry+/ GFAP+mCherry+
AAV9-miR-124
K
3 weeks
% Tbr1+BrdU+mCherry+/ Tbr1+ mCherry+
n.s.
AAV9-miR-124
AAV9-miR-124 +ISX9
L
3 weeks
% Tbr1+BrdU+mCherry+/ mCherry+
n.s.
AAV9-miR-124
AAV9-miR-124 +ISX9
M
mCherry/Tbr1/BrdU/DAPI
3 weeks

1310 **Figure 7: miR-124 induces reprogramming of resident reactive astrocytes to iNs with cortical**
1311 **identity *in vivo* following cortical trauma**

1312 **(A)** Experimental setup for the lentiviral approach. **(B)** LV-124-transduced cells in the
1313 peritraumatic cortical parenchyma expressing the mature neuronal marker NeuN, 3w after
1314 viral transduction. Inset area indicated in white frame. **(C)** Percentage of control LV-GFP and
1315 LV-124-transduced cells expressing NeuN, 7d and 3w post-transduction with or without
1316 treatment with ISX9, (average ± SD, n=4 animals for all groups and time points, **p<0.01). **(D)**
1317 Experimental setup for the AAV approach. **(E)** Percentage of AAV9-miR-124-transduced cells
1318 expressing the astrocytic marker GFAP or the mature neuronal marker NeuN, 7d p.i. (average
1319 ± SD, n=3 animals). **(F)** AAV9-124-transduced cells (in red detected with an anti-RFP antibody)
1320 expressing NeuN, 3w p.i. Inset area indicated in white frame. **(G)** Percentage of AAV9-miR-
1321 124-transduced cells in the peritraumatic parenchyma expressing NeuN at d7, 3w and 8wp.i.
1322 with or without treatment with ISX9, (average ± SD, n=3-4 animals per group, *p<0.05,
1323 **p<0.01 and ***p<0.001). **(H)** Representation of the average number of mCherry+ (blue
1324 bars) and NeuN+/mCherry+ cells (inner gray-blue bars) present in the peritraumatic
1325 parenchyma 3w and 8w p.i. in the presence or absence of ISX9, (average ± SD, n=3 animals
1326 per group per time point, *p<0.05 for the number of NeuN+/mCherry+ cells in AAV9-miR-
1327 124+ISX9 *vs* AAV9-miR-124 at 8w). **(I)** Experimental setup for the BrdU administration. **(J)**
1328 Percentage of GFAP+/mCherry+ cells that have incorporated BrdU 7d p.i. (average ± SD, n=3
1329 animals). Percentage of Tbr1+/mCherry+ cells that originated from a proliferating state
1330 (BrdU+) **(K)** and percentage of mCherry+ cells that originated from a proliferating state and
1331 have undergone reprogramming (Tbr1+/BrdU+) **(L)** 3w p.i. (average ± SD, n=3 animals per
1332 group). **(M)** miR-124-transduced cells (in red detected with an anti-mCherry antibody) in the
1333 peritraumatic parenchyma that express Tbr1 and have incorporated BrdU 3w p.i. Inset area
1334 indicated in white frame.

1335

1336 # Tables

1337 **Table 1:** Sequences of primers for real-time PCR used in this study

Gene	Forward primer	Reverse primer
Mash1	TCTCCGGTCTCGTCCTACTC	CAAAGTCCATTCCCAGGAGA
Neurog2	GTCCCCATACAGCTGCACTT	CAGGTGAGGTGCATAACGGT
Tbr2	CACCCAGAATCTCCTAACACTG	AGCCTCGGTTGGTATTTGTG
Tbr1	TCCAGACGTTCACTTTTCCG	CCCGTGTAGATCGTGTCATAG
Cux1	AGCAGAGACTTTAAGGGAACAG	GCAGCCAACTCTACTTCTAGG
Fezf2	TTTGTGGCAAAGGCTTTCAC	TCTTGTCGTTGTGGGTGTG
Gsx2	GATTCCACTGCCTCTCCATG	CGGGACAGGTACATATTGGAAG
Dlx1	CAGTTCCGTGCAGTCCTAC	ATTGTCCTGGGTTTACGGATC
Sox4	GAACGCCTTTATGGTGTGGT	GAACGGAATCTTGTCGCTGT
Sox11	CCCTGTCGCTGGTGGATAAG	GGTCGGAGAAGTTCGCCTC
Hes6	TACCGAGGTGCAGGCCAA	AGTTCAGCTGAGACAGTGGC
NeuroD1	TTGAAGCCATGAATGCAGAG	TCTTGGGCTTTTGATCATCC
Scrt1	AATCATGCCCAGGTCCTTC	CCACGTAGTCACTGAGGTATC
Lhx6	GACACCATGATCGAGAACCTC	CAATTGCTCTGCGGTGAAG
Chd5	ATCTACGAAATCTGGCACCG	CCCTTGTGGATCTCAGACTTG
En1	CTACTCATGGGTTCGGCTAAC	TCTTTAGCTTCCTGGTGCG
Foxa1	AGGGTTGGATGGTTGTGTC	AGGCCGGAGTTCATGTTG
Lmx1b	CGGGATCGGAAACTGTACTG	AGCAGAAACAGCCCAAGTG
Hoxc4	CAAGCAACCCATAGTCTACCC	AACTCTTTCTCTAATTCCAGGACC
Phox2a	TCCCTTCTCTGGAGTTCTGTC	GATAATGCCAGGTCCAGAAGG
Elavl2	AATAACAGGGCAGAGCTTGG	TCTGATTGAGGCTGAGCTTG
Elavl3	GGTTCGGGATAAGATCACAGG	CAGAACTGGGACGTGCATAG
Elavl4	AGAATCCTGCAAACTCGTGAG	ATGGTTTTGGTCTGGAGTCTG
Nova1	GCTGGCTACCTCTGGATCAT	TGGGATGCCATTTAGCTTGC
Zfp36l1	CACACCAGATCCTAGTCCTTG	CTGGGAGTGCTGTAGTTGAG
Zfp36	TCTCTTCACCAAGGCCATTC	GAGTCCGAGTTTATGTTCCAAAG
Rbpj	TCCCAAAACCCGGATAACC	TTTCGCATAGCTTCCCTAGTG

Tcf7l1	CTACAGCAACGACCACTTCTC	GGTAATACGGTGACAGCTCAG
Tcf4	CACAAACCATTACAGCACCTC	GTGTGGTCAGGAGAATAGATCG
Nfic	GGACGGAAGACATAGAAGGAG	GGGCTGTTGAATGGAGATTTG
Tox	TGCTCTCCAATTCCATCTCTG	CTGTCTGATGTCTGTAGGCTG
Rcor2	GCATGTACCTGAGTCCTGAAG	CTGCTATTGGTCTGCTTCATG
Rbfox1	AGTTACGGACGAGTTTATGCTG	AGAGAACGAGACCCACATCA

1338